Mineralogical and elemental geochemical characteristics of Taodonggou Group mudstone in Taibei Sag, Turpan-Hami Basin: Implication for its formation mechanism

Huan Miao[1,2*], Jianying Guo[3*], Yanbin Wang[4], Zhenxue Jiang[1,2], Chengju Zhang [1,2], Chuanming Li[1,5]

（1. State Key Laboratory of oil and gas resources and exploration, Beijing 102249, China;

2. Institute of unconventional oil and gas science and technology, China University of Petroleum (Beijing), Beijing 102249, China;

3. CNPC Key Laboratory of Natural Gas Accumulation and Development，Langfang 065007，China；

4 School of Geosciences and Surveying Engineering，China University of Mining and Technology（Beijing），Beijing 100083，China；

5. College of Geosciences, China University of Petroleum (Beijing), Beijing 102249, China;)

Corresponding author: Huan Miao1627765379@qq.com; Jianying Guo gjy_17711224@petrochina.com.cn

Abstract: Organic matter types in the Taodonggou Group mudstone exhibit significant differences with depth. In order to understand the formation mechanism of this special phenomenon, we analyzed the mineralogy and geochemistry of the mudstone, as well as the source rocks, depositional environment, and depositional processes of the Taodonggou Group. Based on this, we have gained the following understanding: (1) The Taodonggou Group mudstone was deposited in an intermediate-depth or deep, dyoxic, freshwater-brackish lake environment under warm and humid paleoclimatic conditions. The input of terrestrial debris was stable, but the sedimentation rate was slow. In addition, the sedimentation in the middle stage was influenced by hydrothermal activities, and the changes in the depositional environment corresponded to variations in organic matter types. (2) The source rocks of the Taodonggou Group mudstone are mainly andesitic and feldspathic volcanic rocks. Sediment sorting and recycling were weak, and hydrocarbon source information was well preserved. The tectonic background of the source area was a continental island arc and an oceanic island arc. Furthermore, changes in the provenance of the Taodonggou Group also had a significant impact on the variations in organic matter types. (3) The sedimentation of the Taodonggou Group involved both traction and gravity flows. The variations in source area, depositional environment, and depositional processes during different depositional periods led to changes in the organic matter types of the Taodonggou mudstone. (4) Based on the depositional environment, provenance, and depositional processes, the sedimentation of the Taodonggou Group can be divided into three stages. In the early stages, the sedimentation center was in the Bogda area. At this time, the Bogda Mountain region was not exposed, and the depositional processes inherited the characteristics of Early Permian gravity flow sedimentation, resulting in the widespread deposition of a series of high-quality Type III source rocks in the basin. In the middle stage of the Taodonggou Group sedimentation, the sedimentation center gradually migrated to the Taibei Sag. During this period, the Bogda Mountain region experienced uplift and hydrothermal activity, and the depositional processes gradually transitioned to traction flows, resulting in the widespread deposition of a series of Type II source rocks in the basin. In the late stage of the Taodonggou Group, the uplift of the Bogda Mountain region ceased, and the sedimentation center completely shifted to the Taibei Sag. Meanwhile, under the influence of gravity flows, the organic matter types of the

Taodonggou mudstone changed to Type III.

Keyword: Turpan-Hami Basin；Taodonggou Group；Mineralogy；Element Geochemistry；Sedimentary Environment; Source sink system

1 Introduction

Turpan-Hami Basin, Junggar Basin and Bogda area all belong to the southern part of the ancient Asian ocean in the Paleozoic era (Korobkin and Buslov, 2011; Jiang et al., 2015). During the Early Carboniferous to Early Permian, they began momentously to separate due to the continuous expansion of the Bogda Rift and began to enter the basin-forming period in the Middle Permian (Miao et al., 2004; Novikov, 2013; Jiang et al., 2015; Wang et al., 2019; Zhang et al., 2019). The Middle Permian is a momentous stage in the tectonic evolution of the Turpan-Hami basin. During this period, the expansion of the Bogda Rift stopped. With the gradual withdrawal of seawater from Xinjiang, the sedimentary environment of the Turpan-Hami basin gradually shifted to continental facies, and the sedimentary center gradually shifted from the Bogda area to Taibei Sag (Miao et al., 2004; Shi et al., 2020; Li et al., 2022). Taodonggou Group mudstones are widely deposited in the Turpan-Hami Basin. Previous studies have confirmed that Taodonggou Group mudstone is a very good to excellent source rock with huge hydrocarbon generation potential (Song et al., 2018; Miao et al., 2021; Miao et al., 2022; Miao et al., 2022b). It has been found that the organic matter types of the Taodonggou mudstone can be classified into two categories, with the upper and lower sections being Type III and the middle section being Type II (Miao et al., 2021).

The hydrocarbon generation potential of mudstone is closely related to its sedimentary environment (Wu et al., 2021; Li et al., 2022; Zhang et al., 2019; Zhao et al., 2021; Miao et al., 2004). Regarding the sedimentary environment of the Taodonggou Group mudstone, previous researchers have conducted extensive research. Miao et al. (2004) believed that the mudstone in the Taodonggou Group was deposited in a warm and humid paleoclimate, high-salinity water bodies, and an anoxic environment. Yang et al. (2010), based on the sedimentary characteristics of the Taerlang Formation and the Daheyan Formation, believed that the Taodonggou Group was deposited in a subhumid climate and that climate change is periodic. Wei (2015) also confirmed that the paleoclimate change of the Taodonggou Group stratum has a cyclical feature through tree rings and is mainly a warm and humid paleoclimate. At the same time, Song et al. (2018) also confirmed this by using the elemental geochemical characteristics of the Taodonggou Group shale outcrops in the field; Tian et al. (2017) analyzed the biomarkers of the Taodonggou Group in 7 outcrops around the Turpan-Hami Basin and concluded that the mudstone of the Taodonggou Group was deposited in a balanced, filled lake with little or no terrestrial organic matter, a large amount of algal organic matter input, and weakly alkaline, hypoxic to hypoxic brackish water. Miao et al. (2021) found biomarkers in the Taodonggou Formation mudstone from wells YT1 and L30 from different perspectives of Tian, which may be related to the weathering effect of outcrop samples. Through the research of the above scholars, we have found that there is some

controversy over the sedimentary environment of the Taodonggou Group, and the relationship between the cyclic changes in the sedimentary environment and the changes in the organic matter types of the Taodonggou Group mudstone is still unclear.

In addition, the provenance and sedimentation mode of sediments also have a significant influence on the organic matter types in mudstones (Mei et al., 2020). Mudstone belongs to a category of fine-grained sediment that is challenging to analyze using traditional heavy mineral analysis methods (Rollinson, 1993; Roser and Korsch, 1988; Gehrels et al., 2008). Therefore, elemental geochemical methods can be employed for provenance analysis (McLennan et al., 1983; Kröner et al., 1985; Li et al., 2020). Elemental geochemical analysis compares the major, trace, and rare earth element characteristics of mudstones in the sedimentary area with those of lithologies in the provenance area to determine the lithology of source rocks, weathering degree, and tectonic background of the sediment source area (Li et al., 2020; Floyd and Leveridge, 1987; Basu et al., 2016). Previous studies have found that the sediment source not only affects variations in the salinity of lake water but also influences the input of nutrients and terrestrial organic matter, thus impacting the quality of mudstones (Li et al., 2020; Deditius, 2015; Essefi, 2021). The tectonic activity in the source area not only affects changes in the sedimentary center but also influences the source area (Miao et al., 2022; Pinto et al., 2010). Therefore, reconstructing the location and sedimentation mode of the sediment source area is of great significance for understanding the variations in organic matter types in the Taodonggou Group mudstones.

Based on the mineralogical and elemental geochemical characteristics of 16 mudstone samples collected from the YT1 well, this study aims to reconstruct the paleoclimatic features, provenance, and tectonic background of the sedimentary period in the source area of the Taodonggou Group mudstones. It also aims to explore the influence of sedimentary environment, provenance changes, and sedimentation mode on the deposition of the Taodonggou Group mudstones, in order to reveal the formation process of the mudstones.

2 Geological setting

The Turpan-Hami Basin, located in the eastern part of Xinjiang Uygur Autonomous Region, is one of the three major petroliferous basins in Xinjiang. It is 660 km long from east to west and 130 km wide from north to south, with a total covered area of 5.35×10^4 km². The Turpan-Hami Basin has undergone four stages: the extensional rift basin development stage, the compressional foreland basin development stage, the extensional faulted basin development stage, and the compressional regenerated foreland basin development stage, which finally formed the current pattern of the Mesozoic-Cenozoic superimposed composite inland basin (Zhu et al., 2009; Jiang et al., 2015; Wartes et al., 2002; Greene et al., 2005). According to the tectonic evolution characteristics of the Turpan-Hami Basin, the Turpan-Hami Basin can be divided into three primary tectonic units from east to west: the Hami Depression, the Liaodun Uplift, and the Turpan Depression (Miao et al., 2021; Fig. 1a).

Taibei sag, the secondary sag of Turpan depression in Turpan-Hami basin, is the largest sedimentary unit in Turpan-Hami

批注 [繆欢2]: Based on the comments of Reviewer 1, the introduction has been redesigned and written

3

94 basin (Fig. 1b). The Taibei sag is a Paleozoic-Cenozoic inherited subsidence area (Li et al., 2021), which is a key area for oil

95 and gas exploration in the Turpan-Hami Basin due to its high thermal evolution degree of hydrocarbon source rocks, good

96 reservoir physical properties, good cap sealing, and rich oil and gas resources, which are the focus of oil and gas exploration

97 in the Turpan-Hami Basin. (Wu et al., 2021; Li et al., 2021). Taodonggou Group is the general name of the Daheyan Formation

98 and the Taerlang Formation. The Daheyan Formation is composed of a sequence of sandstone and conglomerate deposits,

99 with locally interbedded gray to dark gray mudstone. It is unconformably overlain by the Yierxitu Formation. The Taerlang

100 Formation is predominantly composed of gray-black mudstone, with localized occurrences of gray-green siltstone and

101 medium-grained sandstone. Due to the fact that the stratigraphic boundary between the Taerlang Formation and the Daheyan

102 Formation is not obvious, they are collectively called the Taodonggou Group. The Middle Permian Taodonggou Group is

103 mainly located in the western part of the study area. At present, only the YT1 and L30 wells are drilled (the YT1 well is drilled

104 through; the L30 well is not drilled through). The burial depth of the stratum is 4000–6500 m, and the thickness of the

105 mudstone is 50–200 m (Miao et al., 2022b).

批注 [缪欢3]: Add the relationship between sandstone and mudstone based on the comments of Reviewer 2

106
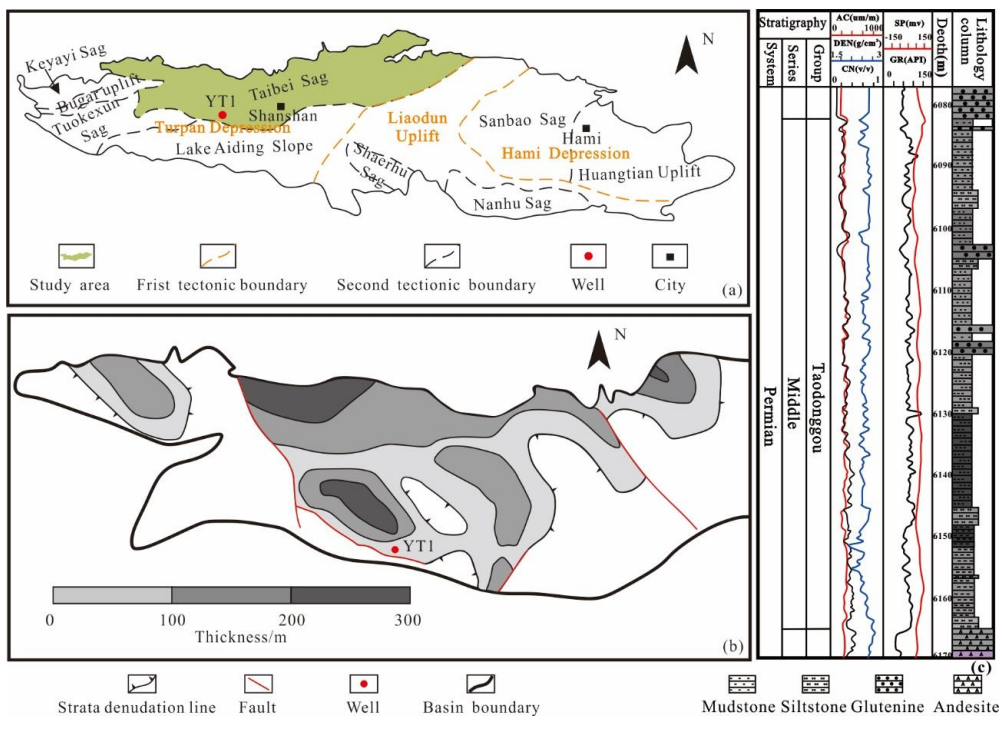
107 Fig.1: Geological overview of the study area (modified after Miao et al., 2021; Miao et al., 2022b): (a) Geological background of Turpan-Hami

108   basin; (b) Thickness contour map of Taodonggou Group mudstone in Taibei sag; (c) YT1 stratum of Taodonggou Group

109 **3 Samples and experiments**

4

3.1 Samples

In this study, 16 mudstone samples were collected from well YT1, numbered YT1-1 to YT1-16 in order of depth. After cleaning the samples, XRD, XRF and ICP-MS experiments were conducted.

3.2 Experiments

The XRD experiment was carried out at Hangzhou Yanqu Information Co., Ltd. The experimental instrument was the Ultima VI XRD testing instrument of Japanese Neo-Confucianism. In accordance with the Chinese industry standard SY/T 5163-2018, the mudstone was broken to a particle size of less than 200 meshes, and 2 g of samples were weighed to obtain XRD images through Cu/Ka radiation at a scanning speed of 2 °/min. The measurement angle range was $3° \leq 2\theta \leq 70°$, and finally, quantitative interpretation is made with the software X'Pert Highscore Plus of Panalytic Company.

The XRF experiment was conducted in Hangzhou Yanqu Information Co., Ltd., and the experimental instrument was a Panalytical Axios tester from Panalytical. The mudstone was first crushed to a particle size of less than 200 meshes, then 10 g of the sample was weighed and calcined in a muffle furnace for 4 hours to get rid of organic matter and carbonates, weighed and recorded the weight loss, and finally $Li_2B_4O_7$ was added, mixed evenly and made into glass bead, and the main element concentration was tested.

The ICP-MS test was performed at Beijing Orient Smart, and the test instrument was an ELEMENT XR inductively coupled plasma emission spectrometer manufactured by Thermo Fisher, Inc. Before analysis, the samples were ground to a particle size of less than 40 μm. An appropriate amount of the sample was weighed and dissolved in HF (30%) and HNO3 (68%) at 190℃ for 24 hours. After evaporating the excess solvent with deionized water, the solution was redissolved in 2 ml of 6.5% HNO_3. Redissolve in 2 ml of 6 mol/L HNO_3 and then store at 150 °C for 48 hours. Subsequently, after evaporating the solution, 1 ml of the 6 mol/L HNO_3 evaporated solution was added to the sample.

4 Results

4.1 Mineralogy

The XRD test results of 16 samples from Well YT1 are shown in Table 1 and Figure 2. As can be seen from Table 1 and Figure 2, Taodonggou Group mudstones are composed of clay, quartz, calcite, plagioclase, barite, and K-feldspar, and some samples contain siderite and pyrite. The content of clay is the highest (23.9%–70.9%, mean 40.78%), followed by quartz (17.2%–59.2%, mean 34.69%), calcite (1%–35.4%, mean 16.97%), barite (0%–13.3%, mean 4.21%), plagioclase (0%–5.4, mean 2.93%), and K-feldspar (0%–2.3, mean 0.9%).

The mineral composition can be used to analyze the lithofacies type of mudstone, and different lithofacies types often have different characteristics (Glaser et al., 2014). Previous scholars believed that mudstone types could be divided by the ternary diagram of mineral composition. The three end elements of the ternary diagram are quartz + feldspar + mica (QFM), calcite + dolomite + ankerite + siderite + magnesite (carbonate), and clay. The XRD results of 16 mudstone samples from Well YT1 in the study area are put into the ternary map (Fig. 3). The results show that the data points of Taodonggou Group

批注 [缪欢4]: Based on the comments of Reviewer 2, modify the symbols

5

142   mudstone in the study area are located in four areas, namely, mixed mudstone, silica-rich argillaceous mudstone, argillaceous

143   siliceous mudstone and mixed siliceous mudstone, and most of the points are mixed mudstone and argillaceous siliceous

144   mudstone areas, which indicates that Taodonggou Group mudstone can be divided into four types: mixed mudstone, silica-

145   rich argillaceous mudstone, argillaceous siliceous mudstone and mixed siliceous mudstone, and the main lithofacies are mixed

146   mudstone and argillaceous siliceous mudstone.
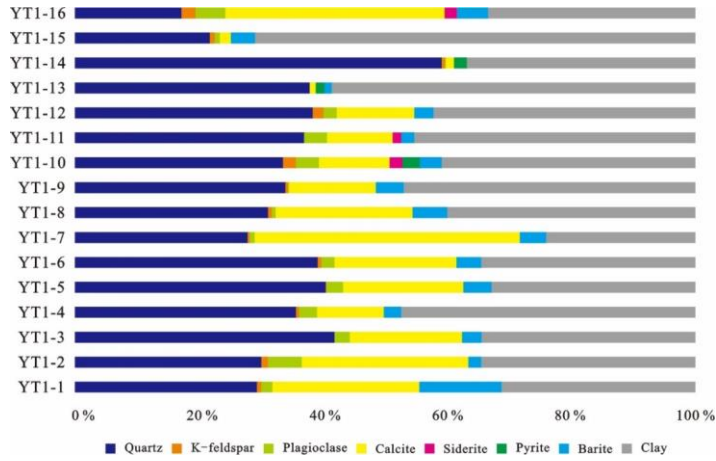
147
148   Fig.2 Mineral composition of Taodonggou group mudstone in YT1 well
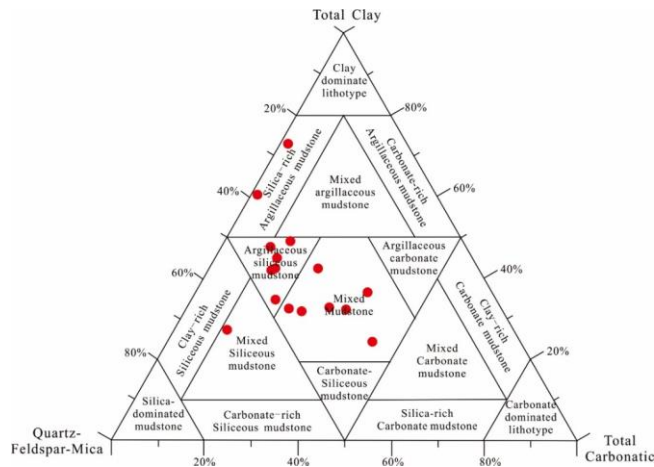
149
150   Fig.3 Lithofacies classification of Taodonggou Group mudstone in well YT1(modified from Glaser et al., 2014)

151 **4.2 Major element**

152   Table 2 shows the results of the major elements in 16 mudstone samples from Well YT1. From Table 2, we can see that

153   the major elements of the Taodonggou Group mudstone are mainly SiO_2, Al_2O_3, Fe_2O_3, CaO, and TiO_2. The highest content

154   of SiO2 is from 43.11% to 70.11%, with an average value of 56.18%. Al_2O_3 content takes second place, accounting for 11.65%

6

155 to 25.75%, with an average value of 18.69%; the average content of another main element is less than 10%.

156 **4.3 Trace element**

157   The trace element content of the Taodonggou Group mudstone is shown in Table 3. Enrichment factor (EF) is an

158 important indicator of element enrichment (Taylor and McLennan, 1985; Ross and Bustin, 2009). By comparing the trace

159 element content of the mudstone of the Taodonggou Group with the global average shale (AS), the trace element enrichment

160 factors in the study area are calculated as follows:

161    $$X_{EF} = \frac{(X \, / \, Al)_{samples}}{(X \, / \, Al)_{AS}} \qquad （1）$$

162   Where X and Al represent the concentrations of elements X and Al (Taylor and McLennan, 1985; Ross and Bustin, 2009).

163 $X_{EF} < 1$ represents the dilution concentration of element X relative to the standard composition, $X_{EF} > 1$ represents the relative

164 enrichment of element X compared to the AS concentration, $X_{EF} > 3$ represents the detectable autogenetic enrichment, and

165 $X_{EF} > 10$ is considered an indicator of moderate to strong autogenetic enrichment (Taylor and McLennan, 1985; Ross and

166 Bustin, 2009).

167   Figure 4 presents the enrichment factors of Taodonggou Group mudstone in the study area. It can be seen from Figure 4

168 that only Hf (1.29) is enriched in the Taodonggou Group mudstone compared with AS, and other elements are not enriched.
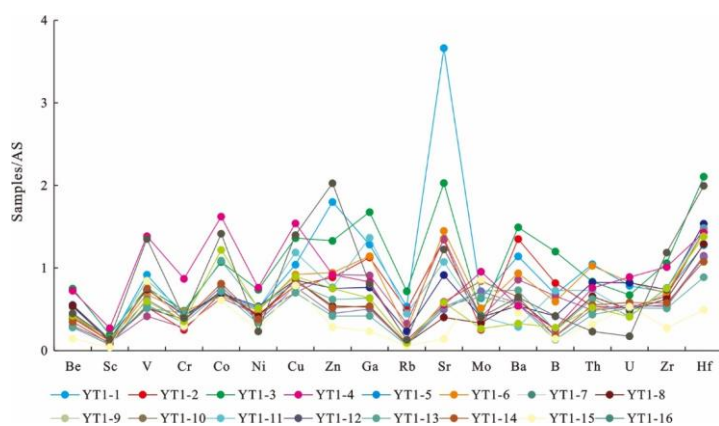
169

170   Figure 4 AS standardized multi-element diagrams of Taodonggou Group mudstone in the study area.

171 **4.4 Rare earth element**

172   The REE content of Taodonggou Group mudstone in the study area is shown in Table 4. According to Table 4, the $\sum$REE

173 content of Taodonggou Group mudstone ranged from 43.247×10^{-6} to 257.997×10^{-6}, with an average value of 159.206×10^{-6}.

174 $^{-6}$. The light rare earth element (LREE) content was the highest (mean value 133.45×10^{-6}), followed by medium rare earth

175 element (MREE) (mean value 17.438×10^{-6}) and heavy rare earth element (HREE) (mean value 6.684×10^{-6}) in that order.

176 After chondrite standardization (Taylor and Mclennan, 1985), Taodonggou Group mudstone shows a right dipping REE

177 distribution pattern (Fig. 5), $(La/Yb)_N$ is 6.228–10.081, with an average value of 7.358.

7
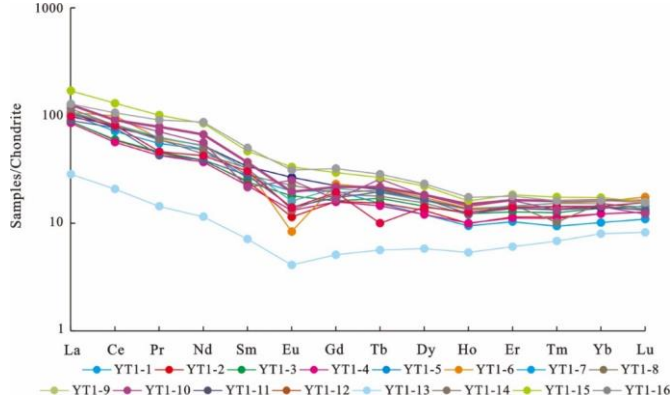
179　　　　　　　　Figure 5. Standardized map of rare-earth element chondrite in mudstone of Taodonggou Group

180 **4.5 Reconstruction of paleosedimentary environment based on element geochemical characteristics**

181 4.5.1 Paleoclimate and weathering

182　　　　The paleoclimate not only affects the weathering degree of the parent rock but also affects the transport distance of

183 sedimentary debris and the transport of nutrients (Zhang et al., 2005). There are many evaluation indices for paleoclimate,

184 such as the chemical alteration index (CIA) and the climate index (C). It is generally believed that when CIA=50–65 and C <

185 0.2, it reflects that the sedimentary system is in a dry and cold climate under the background of lower of degree of chemical

186 weathering; when CIA=65–85 and 0.2 < C < 0.8, it indicates that the sedimentary system is in a warm and humid climate

187 under the background of middle of degree of chemical weathering; when CIA=85–100 and C > 0.8, it reflects the humid and

188 hot climate under the background of high of degree of chemical weathering (Zhang et al., 2019; Nesbitt and Nesbitt, 1984).

189 The calculation formula for CIA and C is as follows:

190　　$CIA = \dfrac{Al_2O_3 \times 100}{Al_2O_3 + Na_2O + CaO^* + K_2O}$　　　（2）

191　　$C = \dfrac{Fe + Mn + Cr + Ni + V + Co}{Ca + Mg + Sr + Ba + K + Na}$　　　（3）

192　　　　In formula (2), CaO * only refers to CaO in silicate minerals. Due to the lack of direct measurement means, it is often

193 calculated indirectly by the content of P_2O_5, namely:

194　　$CaO^* = mol(CaO) - \dfrac{10}{3} mol(P_2O_5)$　　　（4）

195　　　　Where, mol(CaO) and mol(P_2O_5) are the mole numbers of CaO and P_2O_5, where when mol (Na$_2$O) ≤ mol (Cao *), mol

196 (Ca0 *) = mol (Na$_2$O); on the contrary, when mol(Na$_2$O) > mol(CaO*), mol(CaO*)=mol(CaO) (Nesbitt and Young, 1984).

197 The CIA values of the Taodonggou Group mudstone in the study area were calculated based on Equation (2) and Equation

198 (3), ranging from 68.71 to 96.97, with a mean value of 80.17. The climate index (C) is 0.22–2.42 (average = 1.01). The overall

199 paleoclimate was warm, humid, and hot (Fig. 7a). According to Table 2, the relationship between CIA value and depth is

8

批注 [缪欢5]: Based on the comments of Reviewer 1, the format of the paper has been revised and the results from the discussion section have been moved to the results

200   analyzed, and it is found that the CIA value first increases and then decreases with depth, indicating that the Taodonggou

201   Group mudstone was deposited in a warm, humid, and hot paleoclimate and can be divided into three stages.

202   In addition, the cross plot of Ga/Rb and K_2O/Al_2O_3 can also be used to analyze the paleoclimate characteristics during

203   the formation of sedimentary rocks (Lerman and Baccini, 1987; Liu and Zhou, 2007). As shown in the cross plot of Ga/Rb

204   and K_2O/Al_2O_3 (Fig. 7b), almost all points are in the warm/wet area, which indicates that Taodonggou Group mudstone was

205   deposited in a warm and humid paleoclimate.

206   Based on the above analysis, the Taodonggou Group mudstone in the study area was deposited in a warm, humid, and

207   hot paleoclimate. This result is consistent with Miao's indicator result using the biomarker parameter CPI (Miao et al., 2021),

208   indicating that the biomarker parameter CPI can be used to explain the paleoclimate change characteristics of hydrocarbon

209   source rocks with $Ro \leq 1.49$.
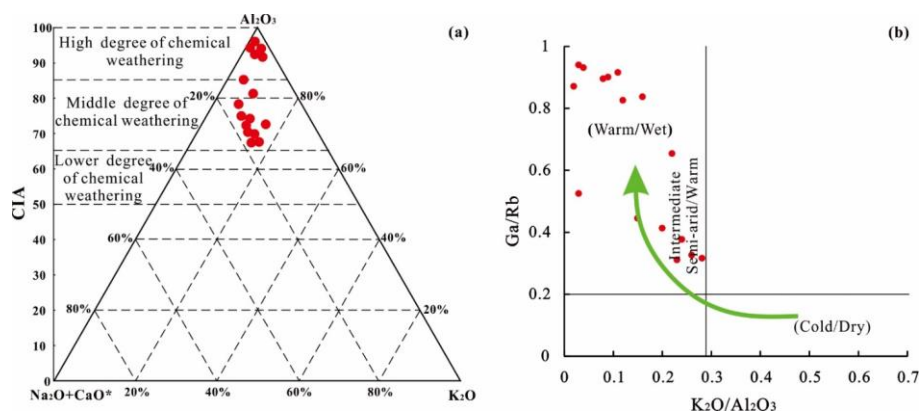
211 Figure.6 Paleoclimate index of Taodonggou Group: (a) CIA Characteristics of Taodonggou Group mudstone (modified from Nesbitt and Young,

212 1984); (b) cross plot of K_2O/Al_2O_3 and Ga/Rb (modified from Roy and Roser, 2013)

213 4.5.2 Paleo-redox conditions

214   Redox environments are critical to the preservation of organic matter in sedimentary rocks, and sensitive elements such

215   as Co, Mo, U, Th, V, Ni, and Cr are commonly used to identify redox conditions in ancient water bodies. Previous evidence

216   suggests that U/Th < 0.75, V/Cr < 2 and V/(V+Ni) < 0.45 represent an oxic conditions, 0.75 < U/Th < 1.25, 2 < V/Cr < 4.25

217   and 0.45 < V/(V+Ni) < 0.84 represent a dyoxic conditions, U/Th < 1.25, V/Cr < 4.25 or V/(V+Ni) < 0.84 represent an anoxic

218   condition (Hatch and Leventhal, 1992; Rosenthal et al., 1995; Tribovillard et al, 2006; Tribovillard et al, 2012). There is no

219   significant correlation between V, U, and Th and Al_2O_3 contents in the Taodonggou Group mudstone samples, indicating that

220   V, U, and Th contents in Taodonggou Group mudstone are mainly controlled by authigenic deposition under redox conditions

221   (Tribovillard et al., 1994). The U/Th, V/Cr, and V/(V+Ni) of the Taodonggou Group mudstone range from 0.21 to 0.52 (mean

222   = 0.29), 1.62 to 4.95 (mean = 2.7), and 0.65 to 0.92 (mean = 0.75). In the light of U/Th, Taodonggou Group mudstones were

批注 [缪欢6]: Based on the opinions of reviewers 1 and 2, correct typos

9

223 deposited in an oxic environment, and according to V/Cr and V/(V+Ni), Taodong Group mudstones were deposited in a

224 dyoxic environment. This is because U/Th cannot accurately identify the redox environment of the sediments under highly

225 weathered conditions (Cao et al., 2021), so V/Cr and V/(V+Ni) were used in this study to identify the redox environment of

226 Taodonggou Group mudstone. The cross plot of V/Cr and V/(V+Ni) shows (Fig. 7) that Taodonggou Group mudstones were

227 deposited in a dyoxic environment.
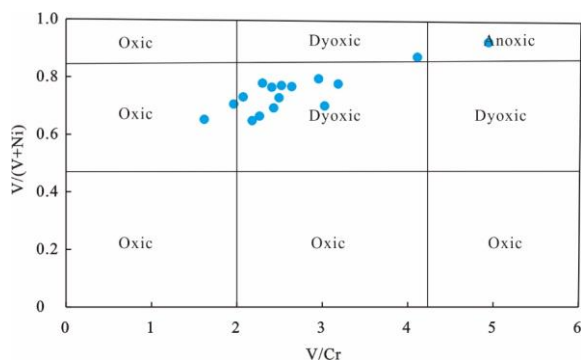
228
229 Figure.7 Cross plot of V/Cr and V/(V+Ni)

230 4.5.3 Paleosalinity

231 Paleosalinity is an important indicator of the paleoenvironment of a water body. The level of paleosalinity affects the

232 stratification of the sedimentary water body and the development of plankton, thereby affecting the paleoproductivity and

233 enrichment of organic matter in the sedimentary environment (Thorpe et al., 2012; Wang et al., 2021; Shi et al., 2021).

234 Previous research has found that Sr/Ba and B/Ga can represent changes in paleosalinity. It is generally believed that Sr/Ba<0.5

235 or B/Ga<3 represents fresh water, 0.5<Sr/Ba<1 or 3<B/Ga<6 means brackish water, and Sr/Ba>1 or B/Ga>6 represents saline

236 water. The correlation between Sr and CaO of Taodonggou Group mudstone in the study area is not obvious (R2=0.17), Sr/Ba

237 of Taodonggou Group mudstone in the study area ranges from 0.32 to 1.83, with an average value of 0.71, and the B/Ga is

238 2.53–5.81 (average = 3.36), indicating that Taodonggou Group mudstone was deposited in freshwater and brackish water

239 environments (Fig. 8a).

240 In addition, Ca/(Ca+Fe) is a reliable indicator for evaluating the salinity of lake waters (Wang et al., 2021). The

241 Ca/(Ca+Fe) distribution of Taodonggou Group mudstone in the study area ranges from 0.14 to 0.78, with a mean value of

242 0.42. The Sr/Ba and Ca/(Ca+Fe) intersection diagram (Fig. 8 b) shows that Taodonggou Group mudstones were deposited in

243 freshwater and brackish water environments, which is in accord with the Sr/Ba and B/Ga intersection diagram.

10
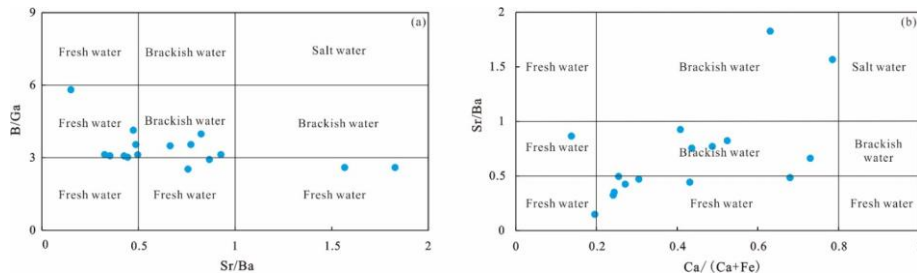
Figure.8 Cross plot of B/Ga and Sr/Ba (a) and cross plot of Ca/(Ca+Fe) and Sr/Ba (b)

4.5.4 Paleobathymetry

Previous research has shown that some elements of the sedimentation process change dramatically with offshore distance. These elements can be used to judge the water depth variation during the sedimentation period. The commonly used indicators are Zr/Al, Rb/K, and MnO content (Xiong and Xiao, 2011; Herkat et al., 2013). It is now believed that the lower the Zr/Al ratio or the higher the Rb/K ratio, the further offshore and the deeper the water (Xiong and Xiao, 2011; Herkat et al., 2013). Zr/Al of Taodonggou Group mudstone is 5.19×10^{-4}– 22.51×10^{-4} (average = 13.44×10^{-4}), showing a trend of first decreasing and then increasing with the depth, Rb/K ranges from 7.32×10^{-4} to 29.79×10^{-4} (mean 19.02×10^{-4}), with large fluctuations with depth of burial. The high-value area of Rb/K is basically consistent with the low-value area of Zr/Al, which indicates that the ancient water depth during the Taodonggou Group mudstone deposition process has a trend of first decreasing and then increasing.

For the content of MnO, it is generally believed that < 0.00094% is a shore lake, 0.00094%–0.0075% is a shallow lake, 0.0075%–0.051% is an intermediate-depth lake, and > 0.051% is a deep lake (Herkat et al., 2013). MnO of Taodonggou Group mudstone is 0.05%–0.30%, with an average of 0.16 %, which indicates that the Taodonggou Group mudstone are mainly deposited in intermediate depth - deep lake sedimentary environment.

4.5.5 Terrigenous detritus input

Ti, Si, and Al are relatively stable during diagenesis and are usually used as indicators of debris flux input (Algeo and Maynard, 2004; Maravelis et al., 2021). Generally, Ti in sediments comes from ilmenite ($FeTiO_3$) or rutile (TiO_2), while Al can exist in feldspar, clay minerals, and other aluminum silicate minerals (Algeo and Maynard, 2004). Compared with Ti and Al, Si comes from many sources, including both biological origin and hydrothermal and terrigenous clastic input (Kidder and Erwin, 2001). Therefore, when using SiO_2 as the evaluation index for terrigenous clastic input, its source needs to be analyzed. The correlation of Al_2O_3 and TiO_2 with SiO_2 in Well YT1 of the study area is not obvious, which indicates that their sources are more complex and not dominated by terrestrial debris sources (Fig. 9). Therefore, Al_2O_3 and TiO_2 are used in this study to indicate the terrestrial debris input during the deposition of the Taodonggou Group mudstone.

The Al_2O_3 content of YT1 wells is higher, ranging from 11.65 % to 25.75 %, with an average value of 18.69 %; the TiO_2

11

270 is 1.15 %–4.22 % (average = 1.77 %). As can be seen from Table 2, the Al_2O_3 content of Well YT1 fluctuates more with depth,

271 and the overall trend is increasing first and then decreasing with depth, while the TiO_2 fluctuates less with depth, and on the

272 whole, the trend is increasing with depth. Combined with the results of paleoclimate analysis in the study area, it is found that

273 the terrestrial debris input during the deposition of the Taodonggou Group strata has the characteristics of increasing first and

274 then decreasing.

275
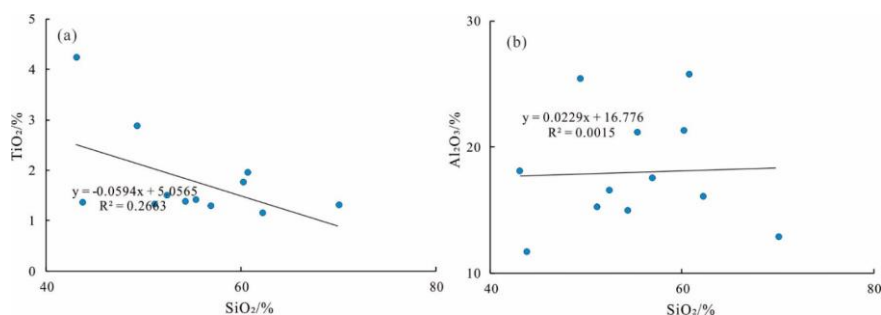
276 Figure.9 Intersection diagram of TiO_2 and SiO_2 (a) and intersection diagram of Al_2O_3 and SiO_2 (b)

277 4.5.6 Paleoproductivity

278 Paleoproductivity determines the quantity of original organic matter in sedimentary rocks (Wei et al., 2012; Algeo and

279 Ingall, 2007; Ross and Bustin, 2009; Schoepfer et al., 2015). The elements P, Si, Ba, Zn, and Cu are indicators of the magnitude

280 of paleoproductivity, but they all have a certain range of application; for example, only the biogenic parts of Si and Ba can

281 represent productivity, and Zn can only represent productivity change in the sulfide reduction environment (Wei et al., 2012;

282 Algeo and Ingall, 2007).

283 P is not only a key nutrient element in biological metabolism but also an important component of many organisms, so it

284 can also be used to characterize biological productivity (Kidder and Erwin, 2001). P/Ti or P/Al is commonly used to reflect

285 biological productivity in order to eliminate the influence of terrigenous detritus. The P/Ti of Taodonggou Group mudstone

286 in the study area ranges from 0.04 to 0.74 percent, with an average value of 0.17 percent and an overall low productivity. As

287 shown in Table 2, the relationship between P/Ti and depth was analyzed, and the results showed that the paleontological

288 productivity tended to increase and then decrease with depth.

289 In addition, Cu is also an important nutrient and, unlike P, is generally indicative of productivity, including the sum of

290 primary productivity and productivity from terrestrial inputs (Schoepfer et al., 2015). For the purpose of eliminating the

291 dilution interference of terrigenous detritus, Cu/Ti is used as an indicator to evaluate the paleoproductivity in this study. The

292 distribution range of Cu/Ti of Taodonggou Group mudstone in the study area is from 0.55 to 1.96 with an average value of

293 1.02 and gradually decreases with depth, indicating a gradual increase in palaeoproductivity during the deposition of

294 Taodonggou Group mudstone.

批注 [缪欢7]: Revise the drawings based on the comments of Reviewer 2

295 4.5.7 Deposition rate

296   The deposition rate is one of the parameters characterizing the magnitude of the dilution effect during deposition and is

297 commonly characterized by $(La/Yb)_N$. It is generally believed that the difference between LREE and HREE migration is not

298 significant when the sedimentation rate of the lake basin is faster and the $(La/Yb)_N$ value is close to 1. Conversely, when the

299 $(La/Yb)_N$ value is greater or less than 1, it indicates that the sedimentation rate of the lake basin is slower (Wang et al., 2021;

300 Cao et al., 2018). The $(La/Yb)_N$ of the Taodonggou Group mudstones are 6.228–10.081, with an average value of 7.358 in the

301 study area, which is much greater than 1. This indicates that the mudstone of the Taodonggou Group has a slower deposition

302 rate.

303 4.5.8 Hydrothermal activity

304   The study area has been extremely volcanically active from the Carboniferous to the Permian, with extensive volcanic

305 deposits in the Middle Permian Taodongou Group, the Lower Permian Yierxitu Formation, and the Carboniferous. In order

306 to explore whether hydrothermal activity is involved in the Middle Permian sedimentation, the Zn-Ni-Co ternary diagram and

307 the $(Cu+Co+Ni)\times10$-Fe-Mn ternary diagram are applied in this study (Xu et al., 2022; You et al., 2019). Based on the Zn-Ni-

308 Co ternary diagram (Fig. 10a), some data points of the Taodonggou Group mudstone are distributed in the hydrothermal

309 sedimentary zone, and based on the $(Cu+Co+Ni)\times10$-Fe-Mn ternary diagram (Fig. 10b), all data points of the samples fall in

310 the hydrothermal sediment zone and Red Sea hydrothermal sediment zone, which indicates that the Taodonggou Group

311 mudstone deposition was influenced by hydrothermal fluids.
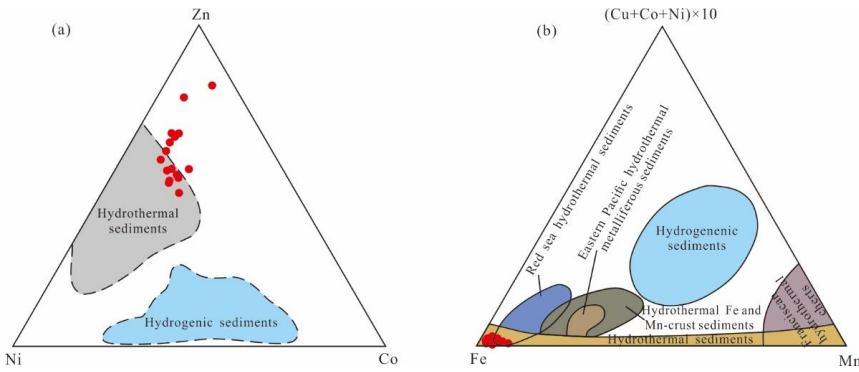
312
313   Fig.10 Zn-Ni-Co ternary diagram (a) and $(Cu+Co+Ni)\times10$-Fe-Mn ternary diagram (b) (modified after You et al., 2019)

314 4.5.9 Tectonic setting

315   Sedimentary rocks of different tectonic settings have prominent differences in element composition and content, so the

316 geochemical characteristics of sedimentary rocks can be used to reflect the tectonic setting of sedimentary basins

317 (Kroonenberg, 1992).

318   The elements Co, Th, Sc, Zr, and La are relatively stable and less affected by geological activities such as weathering,

319 transportation, and deposition. Therefore, the La-Th-Sc ternary diagram and the Th-Co-Zr/10 ternary diagram can be utilized

13

320　to distinguish the tectonic setting during the formation of sediments (Bhatia and Crook, 1986; Cai et al., 2022). Based on the

321　La-Th-Sc ternary diagram (Fig. 11a), most of the data points fall in the continental island arc region, and on the Th-Co-Zr/10

322　ternary diagram (Fig. 11b), almost all the data points fall in the continental island arc and oceanic island arc regions. This

323　indicates that the tectonic setting of the Taodonggou Group's source area is a continental island arc and an oceanic island arc.

324　　　Additionally, previous studies have shown that SiO_2, TiO_2, Al_2O_3/SiO_2 and Fe_2O_3+MgO are also important parameters

325　for identifying the source tectonic setting. Cross plots of Al_2O_3/SiO_2 and Fe_2O_3+MgO, TiO_2 and Fe_2O_3+MgO, and SiO_2 and

326　Al_2O_3/SiO_2 are often employed to recognize the tectonic setting (Bhatia, 1983; Li et al., 2020; Roser and Korsch, 1988). Based

327　on the cross plot of Al_2O_3/SiO_2 and Fe_2O_3+MgO (Fig. 11c), all data points are distributed around the continental island arc

328　and oceanic island arc, which is consistent with the cross plot of TiO_2 and Fe_2O_3+MgO (Fig. 11d) and the cross plot of SiO_2

329　and Al_2O_3/SiO_2 (Fig. 11e). As a result, the tectonic setting of Taodonggou Group mudstone source area is continental island

330　arc and oceanic island arc.

331
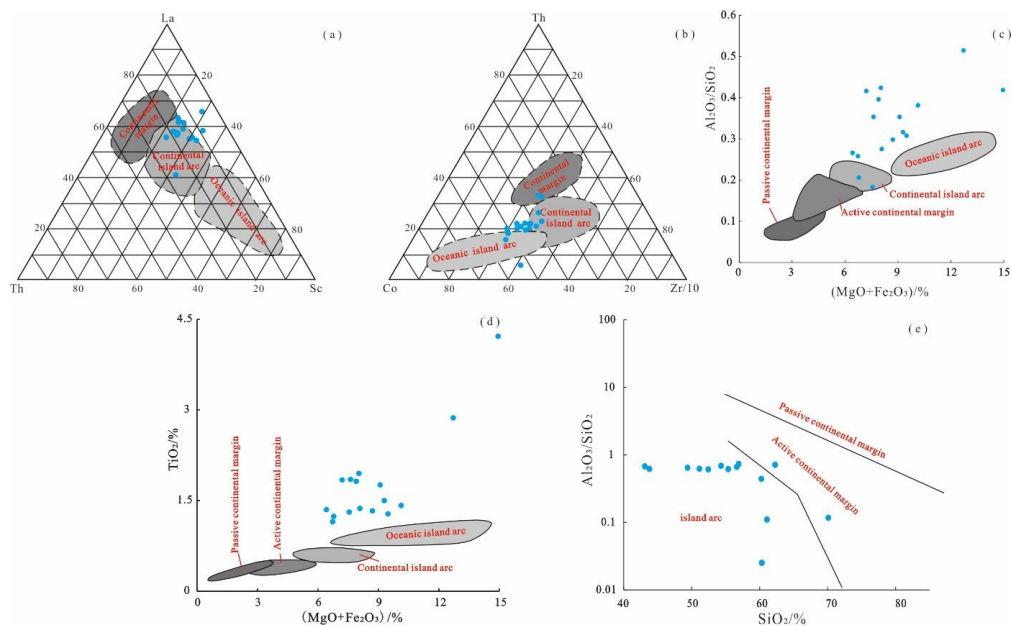
332　Fig.11 Tectonic setting of source area in Taodonggou Group mudstone: (a) La-Th-Sc ternary diagram (modified after Zhu et al., 2021); (b) Th-

333　Co-Zr/10 ternary diagram (modified after Zhu et al., 2021); (c) cross plot of Al_2O_3/SiO_2 and Fe_2O_3+MgO (modified after Bhatia, 1983); (d) cross

334　plot of TiO_2 and Fe_2O_3+MgO (modified after Bhatia, 1983); (e) cross plot of SiO_2 and Al_2O_3/SiO_2 (modified after Roser and Korsch, 1988)

335　**5 Discussion**

336　　　The sedimentary environment, provenance location, and sedimentation mode are factors that influence the quality of

337　mudstones. In this study, based on the mineralogical and elemental geochemical characteristics of the Taodonggou Formation

14

338 mudstones, we discuss the influence of sedimentary environment, provenance location, and sedimentation mode on the quality

339 of the Taodonggou Group mudstones.

5.1 The influence of palaeosedimentary environment on the quality of mudstone

341   Based on the mineralogical, elemental geochemical characteristics and previous studies on the organic geochemical

342 characteristics of the Taodonggou Group mudstones (Miao et al., 2021), a comprehensive geochemical profile of the YT1

343 well was established. The results are shown in Figure 12. It can be observed from Figure 12 that the sedimentary environment

344 of the Taodonggou Group mudstones is closely related to their organic matter types and can be divided into three periods. In

345 the early stage of the Taodonggou Group, the overall climate was warm and humid under moderate chemical weathering

346 conditions. The sedimentary water body was dyoxic-anoxic brackish water. At this time, productivity was weak, and organic

347 matter was mainly derived from terrestrial sources. In the middle stage of the Taodonggou Group, the paleoclimate gradually

348 shifted to a dry and humid climate under strong chemical weathering conditions, accompanied by hydrothermal activity. This

349 provided abundant nutrients for the growth of algae and other microorganisms. At the same time, the sedimentation rate

350 increased, resulting in a predominance of algae in the organic matter composition during this period. During the late stage of

351 the Taodonggou Group, the climate again shifted to a warm and humid climate under moderate chemical weathering

352 conditions. The sedimentation rate slowed down, and the input of organic matter shifted back to predominantly terrestrial

353 sources.

Figure.12 The geochemical profile of the Taodonggou Group in YT1 well

5.2 Provenance

5.2.1 Lithology of parent rock

358   Previous studies have found that the chemical composition of the rocks in the sedimentary area and the parent rock in

359 the provenance area have a strong affinity, and the type of parent rock will directly affect the elemental geochemical

15

批注 [缪欢8]: Based on the comments of reviewers 2 and 3, add parameters such as HI

characteristics of the sediment (Tribovillard et al., 2006; Shi et al., 2021; McLennan et al., 1993; Basu et al., 2016; Hu et al., 2021; Floyd and Leveridge, 1987; Wronkiewicz and Condie, 1987). Generally speaking, the transport of sediment from the source area to the sedimentary area goes through multiple complex processes such as mechanical transport and chemical action, and hence it is necessary to analyze the impact of sediment sorting and recycling on each chemical component when identifying the source. Previous studies have shown that trace elements Zr, Th, and Sc are relatively stable in geological processes such as weathering, transportation, and sorting and are not easily lost, which can be used as one of the indicators for parent rock identification (Floyd and Leveridge, 1987; Wronkiewicz and Condie, 1987). According to the Th/Sc and Zr/Sc intersection diagram of Taodonggou Group mudstone (Fig. 13a), Taodonggou Group mudstone is close to andesite and felsic volcanic rock of the upper crust, and its composition is controlled by the composition of its felsic parent rock and has not undergone sediment sorting and recycling.

In addition, REE and trace elements in mudstone from different parent rocks are obviously different, so the ratio of REE to trace elements can be used to analyze the type of parent rock, and the most common ones are La/Sc, La/Co, Th/Sc, Th/Co, and Cr/Th (Basu et al., 2016; Hu et al., 2021; Floyd and Leveridge, 1987; Wronkiewicz and Condie, 1987; Allègre and Minster, 1978). Based on the Hf and La/Th intersection diagrams (Fig. 13b) and the La/Sc and Co/Th intersection diagrams (Fig. 13c), we can see that the mudstones of the Taodonggou Group have both andesitic island-arc sources and felsic volcanic sources. It can be seen from the cross plot of TiO_2 and Zr (Fig. 13d) that the mudstone of the Taodonggou Group is a source of intermediate igneous rocks and felsic igneous rocks. As can be seen from the cross plot of La/Yb and Σ REE (Fig. 13e), almost all data points are located in the sedimentary rock, alkali basalt, and granite areas.

In summary, the parent rocks of the Taodonggou Group mudstone are andesitic and feldspathic volcanic rocks with weak sedimentary sorting and recirculation, and the material source information is well preserved.
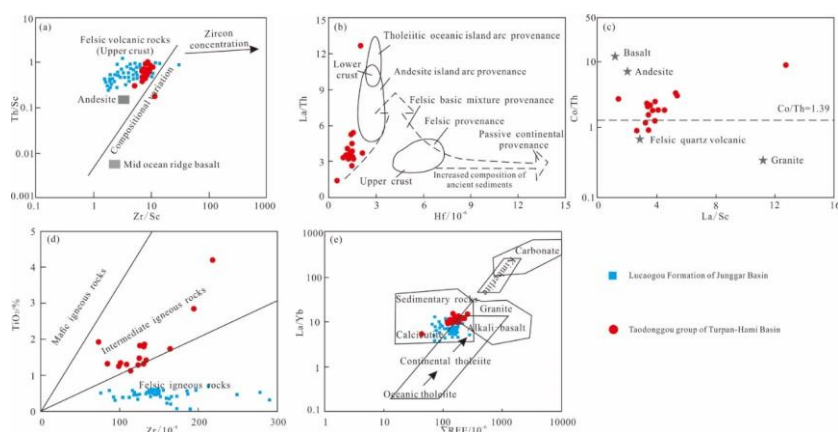
Figure.13 Parent rock type of Taodonggou Group in YT1 well (Data of Lucaogou Formation in Junggar Basin are from Li et al., 2020): (a) Th/Sc

16

and Zr/Sc intersection diagram(modified after Floyd and Leveridge, 1987); (b) La/Th and Hf intersection diagram(modified after Floyd and Leveridge, 1987); (c) Co/Th and La/Sc intersection diagram(modified after Wronkiewicz and Condie, 1987); (d) TiO$_2$ and Zr intersection diagram; (e) La/Yb and ∑REE intersection diagram (modified after Allègre and Minster, 1978)

5.2.2 Location of Parent Rock

There is a great deal of controversy about the provenance location of the Middle Permian in Turpan-Hami (Shao et al., 2001; Jiang et al., 2015; Wang et al., 2019; Zhao et al., 2020; Song et al., 2018; Wang et al., 2018; Tang et al., 2014). Shao et al. (1999) believed that the provenance of the Permian was mainly from the Jueluotage Mountain in the south of the Turpan-Hami Basin; Song et al. (2018) considered that it came from the Bogda area; Zhao et al. (2020) believed that the provenance of the Permian in the Turpan-Hami Basin was consistent with that in Junggar and originated from the Kelameili Mountain and the Northern Tianshan. Summarizing the previous research results, it is found that the main controversial point is the time of the first uplift of Bogda Mountain.

At present, there are many opinions about the time of the Bogda Mountain uplift. They think that the initial uplift of Bogda Mountains occurred in Early Permian (Carroll et al., 1990; Shu et al., 2011; Wang et al., 2018; Li et al., 2022), Middle Permian (Zhang et al., 2006; Liu et al., 2018; Wang et al., 2018), Late Permian-Early Triassic (Zhao et al., 2020; Guo et al., 2006; Wang, 1996; Sun and Liu, 2009; Tang et al., 2014; Wang et al., 2018), Middle Triassic (Guo et al., 2006), Early Jurassic (Green et al., 2005; Liu et al., 2017; Ji et al., 2018) and Late Jurassic (Yang et al., 2015). If the initial uplift of the Bogda Mountains was after the middle Permian, the parent rock types of the Taodonggou Group mudstone in the Turpan-Hami Basin and the Luchaogou Formation mudstone in the Junggar Basin should be the same.

批注 [缪欢10]: Based on the comments of Reviewer 2, the stratigraphic abbreviation has been deleted

We have counted the element geochemical characteristics of Luchaogou Formation in the Junggar Basin (Li et al., 2020) and found that the parent rock type of Luchaogou Formation mudstone in the Junggar Basin is greatly different from that of P$_2$td, which is felsic volcanic rock (Fig. 14). As a result, Bogda Mountain's initial uplift should be Late Permian-Early Triassic in the Early Permian or Middle Permian. This is consistent with Li et al. (2022) and Wang et al. (2018), who inferred the uplift of Bogda Mountain at 289.8 Ma–265.7 Ma. Shao et al. (2001) believed that the sandstone of the Daheyan Formation in Turpan-Hami Basin has a good affinity with the Early Permian and Carboniferous, so the provenance direction of the sandstone of the Daheyan Formation is consistent with that of the Early Permian, and they all come from the Jueluotage Mountain. However, the paleocurrent direction of the Early Permian in Xinjiang is southeast (Zhang et al., 2005; Li et al., 2007; Wang et al., 2019), and the provenance area is located in the north of the Bogda area. Zhao et al. (2020) calculated the U-Pb dating results of 5250 zircons in the Tianshan and believed that the provenance of the Turpan-Hami Basin and the Junggar Basin both came from the northern Tianshan and the Kelameili Mountain, which is also consistent with the ancient ocean current direction in the Early Permian (Zhang et al., 2005; Li et al., 2007; Wang et al., 2019; Fig. 14a). Consequently, the first uplift of Bogda Mountain should have occurred in the early Permian, but it was not exposed in the early Middle

413 Permian, and it still received sedimentation. In the middle Permian, the exposed water began to be denuded, becoming the

414 source area of the Turpan-Hami Basin (Wang et al., 2018).

415   Based on the above analysis, in the early Middle Permian, although Bogda Mountain in the north of Turpan-Hami Basin

416 was uplifted due to orogeny, it did not emerge from the water surface, and it still accepted the provenance of North Tianshan

417 and Kelameili Mountain. At this time, there was a NE-trending ancient ocean current (Carrollet et al., 1995; Obrist-Farnert et

418 al., 2015; Zhao et al., 2020), so Jueluotage Mountain, which has been uplifted in the south of Turpan-Hami Basin, became a

419 secondary provenance area (Shao et al., 1999; Fig. 14b). With the continuous uplift of Bogda Mountain, the sedimentary

420 center of Turpan-Hami Basin gradually shifted to Taibei Sag, and the provenance area of Turpan-Hami Basin changed to

421 Bogda Mountain and Jueluotage Mountain (Fig. 14c).
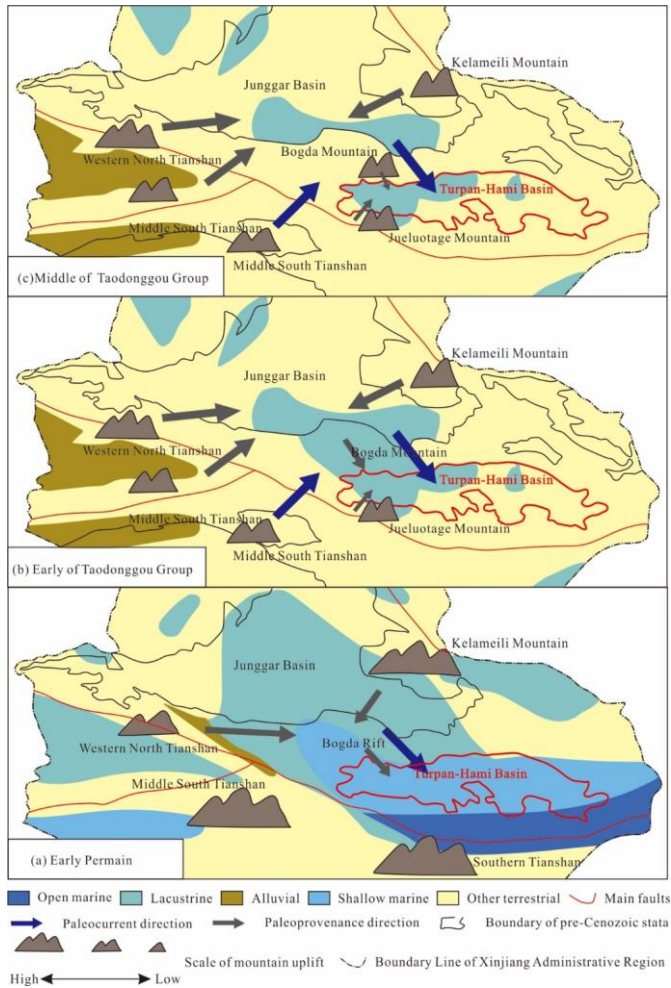
422

Figure. 14 Provenance location from Early Permian to Middle Permian in Tianshan area (modified after Zhao et al., 2020): (a) Early Permian; (b) Early of Taodonggou Group; (c) Middle to later of Taodonggou Group

5.3 sedimentation mode

In previous studies, scholars have believed that the sedimentation of the Permian in the Turpan-Hami Basin is mainly controlled by traction currents (Chen et al., 2003). However, recent research has revealed the presence of gravity flow deposits in the Permian of the Turpan-Hami Basin (Wang et al., 2017; Wang et al., 2018; Xu, 2022). Yang et al. (2010) found poorly sorted debris flow deposits in the Daheshan Formation, and Xu (2022) discovered alluvial and fluvial facies in the Daheshan Formation, consisting of volcaniclastic rocks and conglomerates that are similar in composition to the Lower Permian volcaniclastic rocks and conglomerates. This suggests the existence of gravity flow deposits during the early Permian in the Turpan-Hami Basin. Wang et al. (2018) also suggested the development of gravity flow deposits and pillow lavas in the Early Permian. Meanwhile, in the early Middle Permian, the sedimentation inherited the provenance and sedimentation style from the early Permian, but the gravity flow deposits transitioned gradually into traction current deposits. Due to the influence of gravity flow deposits, terrestrial organic matter can be transported to the deep lake area (Yu et al., 2022; Li et al., 2011), thereby altering the type of organic matter.

During the middle of the Taodonggou Group, the Turpan-Hami Basin entered the foreland basin sedimentation stage due to the uplift of the Bogda Mountains. The sedimentary environment of the Taodonggou Group in the Tainan Sag is similar to that in the Taibei Sag (Li, 2019). During this time, the sedimentary water body of the Taodonggou Group in the Turpan-Hami Basin became shallower, and the dominant sedimentation style transitioned to traction currents. Xu (2022) conducted lithological observations on the Taerlanggou section, the Zhaobishan section, and the Y well in the Taodonggou Group and found the presence of traction structures of gravity flow origin in the middle and upper parts of the Taerlang Formation. Additionally, a large number of calcareous and iron nodules appeared in the formation, indicating the occurrence of gravity flow deposits during the late-stage sedimentation of the Taodonggou Group. The organic matter type in the mudstones during this period was influenced by gravity flows.

5.4 Formation mechanism of the Taodonggou Group mudstone

Based on the sedimentary environment, provenance, and sedimentation mode during the deposition of the Taodonggou Group mudstones, this study has constructed the formation mechanism of the Taodonggou mudstones. The results indicate that the formation of the Taodonggou Group mudstones can be divided into three stages.

In the early of the Taodonggou Group, Bogda Mountain began to rise but did not emerge from the water surface. The sediment source is mainly from North Tianshan and Kelameili Mountain, and the secondary source area is Jueluotage Mountain in the south of the Turpan-Hami basin. The stratum of the Taodonggou Group was deposited in a warm and humid paleoclimate with high weathering intensity and a stable input of terrigenous detritus. In addition, the sedimentary water body is deep at this time, creating a deep lake environment of brackish water and dyoxic. However, this period inherited the gravity

19

批注 [缪欢11]: Add legend based on reviewer 2's comments

批注 [缪欢12]: Based on the comments of Reviewer 3, add and discuss whether there is gravity flow sedimentation in the study area

flow sedimentation characteristics from the Early Permian. Due to the influence of gravity flows, terrestrial organic matter was transported to the deep lake, resulting in the input of organic matter in the mudstones primarily derived from terrestrial higher plants (Miao et al., 2021). Consequently, a high-quality Type III organic matter source rock was formed (Fig.15a).

In the middle of the Taodonggou Group, with the continuous uplift of Bogda Mountain and hydrothermal activity, the climate changed into a hot and humid paleoclimate, the weathering degree further increased, and the input of terrigenous detritus increased. The provenance areas are Bogda Mountain and Jueluotage Mountain. In addition, during this period, the sedimentary center gradually transferred to the Taibei sag, and the sedimentary water body became shallow, which was a dyoxic intermediate-depth lake environment. Due to the nutrients brought by hydrothermal activities, the lower algae multiplied during this period, and the salinity of the sedimentary water body became lower, becoming a freshwater environment and thus depositing a set of high-quality II$_2$ organic source rocks.

In the late Taodonggou Group, the uplift of Bogda Mountain basically stopped, and the climate changed to a warm and humid paleoclimate again. The weathering degree was high, and the input of terrigenous debris was reduced. Bogda Mountain and Jueluotage Mountain remained the provenance areas. The sedimentary center was essentially transferred to the Taibei Sag at this time. During this period, the salinity of the sedimentary water body was high, and the sedimentary water body became deeper. It was a deep lake environment with dyoxic and brackish water. During this period, the sedimentation was also influenced by gravity flows, leading to changes in lithology and organic matter type. As a result, the organic matter type in the mudstones deposited during this period transitioned to Type III.
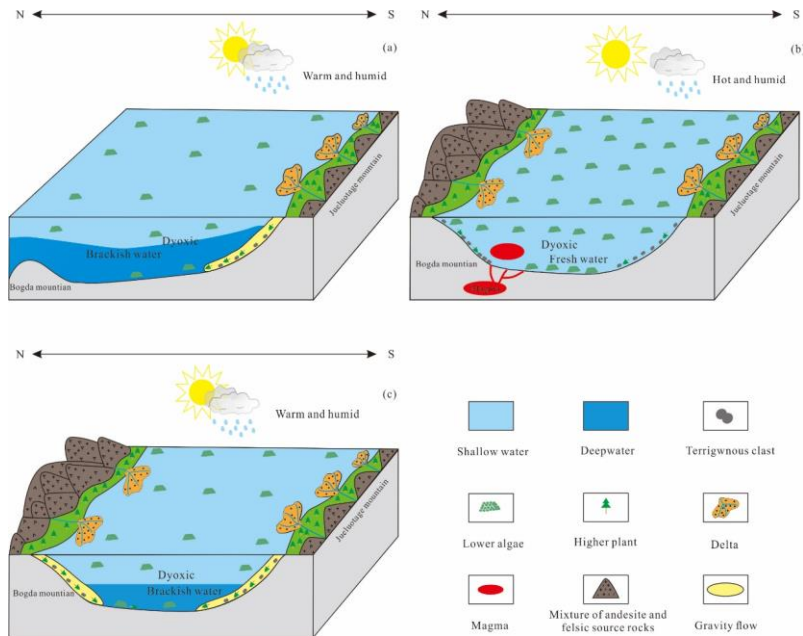
Figure 15 Middle Permian source sink system and lake basin evolution history of Turpan-Hami basin: (a) Early Taodonggou Group; (b) Middle Taodonggou Group; (c) Late Taodonggou Group

6 Conclusion

Through the mineral composition and element geochemistry analysis of the Taodonggou Group mudstone, the following understandings have been obtained:

(1) The mudstone minerals of the Taodonggou Group are mainly clay and quartz and can be classified into 4 petrographic types according to their mineral fractions.

(2) The Taodonggou Group mudstone was deposited in an intermediate-depth or deep, dyoxic, freshwater-brackish lake environment under warm and humid paleoclimatic conditions. The input of terrestrial debris was stable, but the sedimentation rate was slow. In addition, the sedimentation in the middle stage was influenced by hydrothermal activities. In addition, the source rocks of the Taodonggou Group mudstone are mainly andesitic and feldspathic volcanic rocks. Sediment sorting and recycling were weak, and hydrocarbon source information was well preserved. The tectonic background of the source area was a continental island arc and an oceanic island arc.

(3) The sedimentary environment, sources, and sedimentary methods have significant impacts on the organic matter types of the Taodonggou Group. In the early taodonggou Group, the sedimentation center was in the Bogda area. At this time, the Bogda Mountain region was not exposed, and the depositional processes inherited the characteristics of Early Permian gravity flow sedimentation, resulting in the widespread deposition of a series of high-quality Type Ⅲ source rocks in the basin. In the middle taodonggou Group, the sedimentation center gradually migrated to the Taibei Sag. During this period, the Bogda Mountain region experienced uplift and hydrothermal activity, and the depositional processes gradually transitioned to traction flows, resulting in the widespread deposition of a series of Type Ⅱ source rocks in the basin. In the late taodonggou Group, the uplift of the Bogda Mountain region ceased, and the sedimentation center completely shifted to the Taibei Sag. Meanwhile, under the influence of gravity flows, the organic matter types of the Taodonggou mudstone changed to Type Ⅲ.

Data availability

Data will be made available on request.

Acknowledgement

504 **Author contribution**

505　Miao H. and Guo J.Y. designed experiments, Wang Y.B. and Jiang Z.X. revised the first draft of the manuscript, Guo J.

506 Y., Wang Y.B. and Jiang Z.X. provided financial support, Miao H. and Zhang C.J. provided language services and figure

507 production, Li C.M. investigated and revised the ideas of the article, and Miao H. prepared the manuscript with your

508 contributions. All authors contributed to the review of the manuscript.

509 **Competing interests**

510　The contact author has declared that none of the authors has any competing interests.

511 **References**

512 Algeo, T.J.; Ingall, E., 2007. Sedimentary Corg:P ratios, paleocean ventilation, and Phanerozoic atmospheric pO2.

513 Palaeogeogr. Palaeoclimatol. Palaeoecol. 256 (3–4), 130–155.

514 Algeo, T. J.; Maynard, J. B., 2004. Trace-element behavior and redox facies in core shales of Upper Pennsylvanian Kansas-

515 type cyclothems. Chem. Geol. 206(3-4), 289-318.

516 Allègre, C. J.; Minster, J. F., 1978. Quantitative models of trace element behavior in magmatic processes. Earth Planet. Sci.

517 Lett. 38, 1–25,

518 Basu, A.; Bickford, M. E.; Deasy, R., 2016. Inferring tectonic provenance of siliciclastic rocks from their chemical

519 compositions: A dissent. Sediment. Geol. 336, 26−35.

520 Bhatia, M. R., 1983. Plate tectonics and geochemical composition of sandstones. J. Geol. 91, 611– 627.

521 Bhatia, M. R.; Crook, K. A. W., 1986. Trace element characteristics of graywackes and tectonic setting discrimination of

522 sedimentary basin. Contrib. Mineral. Petrol. 92, 181–193.

523 Cai, Y. L. ; Ouyang, F.; Luo, X. R.; Zhang, Z. L.; Wen, M. L.; Luo, X. N.; Tang, R., 2022. Geochemical Characteristics and

524 Constraints on Provenance, Tectonic Setting, and Paleoweathering of Middle Jurassic Zhiluo Formation Sandstones in the

525 Northwest Ordos Basin, North-Central China. Minerals 12(5), 603.

526 Cao, L.; Zhang, Z. H.; Zhao, J. Z.; Jin, X.; Li, H.; Li, J. Y.; Wei, X. D., 2021. Discussion on the applicability of Th/U ratio for

527 evaluating the paleoredox conditions of lacustrine basins. International Journal of Coal geology. 248, 103868.

528 Cao, J.; Yang, R. F.; Yin, W.; Hu, G.; Bian, L. Z.; Fu, X. G., 2018. Mechanism of Organic Matter Accumulation in Residual

529 Bay Environments: The Early Cretaceous Qiangtang Basin, Tibet. Energy & Fuels 32(2), 1024-1037.

530 Carroll, A.; Graham, S.; Hendrix, M.; Ying, D.; Zhou; D..1995. Late Paleozoic tectonic amalgamation of northwestern China:

531 sedimentary record of the northern Tarim, northwestern Turpan, and southern Junggar basins.Geol. Soc. Am. Bull. 107, 5,

532 571-594.

533 Carroll, A.; Liang, Y. H.; Graham, S.; Xiao, X. H.; Hendrix, S.; Chu, J. C.; McKnight, L., 1990. Junggar basin, northwest

534 China: trapped Late Paleozoic Ocean. Tectonophysics 181, 1–14.

22

535 Chen. X., Niu, R.J., Cheng, J.H., 2003. The Sequence stratigraphy of Middle Permian-Triassic in Turpan-Hami Basin.

536 Xinjiang Pet. Geol. 24, 6, 494-497.

537 Deditius, A., 2015. Arsenic Environmental Geochemistry, Mineralogy, and Microbiology. Reviews in Mineralogy and

538 Geochemistry, vol 79. Economic Geology, 110, 7, 1905-1907.

539 Essefi, E., 2021. Geochemistry and mineralogy of the sebkha Oum El Khialate evaporites mixtures, southeastern Tunisia.

540 Resource Geology, 71, 3, 242-249.

541 Floyd, P. A.; Leveridge, B. E., 1987. Tectonic environment of the Devonian Gramscatho Basin, South cornwall: framework

542 mode and geochemical evidence from turibiditic sandstones. Journal of the Geological Society, 144, 4, 531-542.

543 Gehrels, G. E.; Valencia, V. A.; Ruiz, J., 2008. Enhanced precision, accuracy,efficiency, and spatial resolution of U-Pb ages

544 by laser ablation-multicollector-inductively coupled plasma-massspectrometry. Geochem., Geophys., Geosyst. 9, 3, 1– 13.

545 Glaser, K. S.; Miller, C. K.; Johnson, G. M.; Kleinberg, R. L.; Pennington, W. D., 2014. Seeking the sweet spot: Reservoir

546 and completion quality in organic shales. Oilfield Review 25, 16–29.

547 Greene, T. J.; Carroll, A. R.; Wartes, M.; Graham, S. A .; Wooden, J. L., 2005. Integrated provenance analysis of a complex

548 orogenic terrane: Mesozoic uplift of the Bogda Shan and inception of the Turpan-Hami Basin, NW China. Journal of

549 Sedimentary Research 75, 20, 251-267.

550 Guo, Z.; Zhang, Z.; Wu, C.; Fang, S.; Zhang, R., 2006. The Mesozoic and Cenozoic exhumation history of Tianshan and

551 comparative studies to the junggar and Altai mountains Acta Geol. Sin. 80, 1, 1-15

552 Hatch, J.R.; Leventhal, J.S., 1992. Relationship between inferred redox potential of the depositional environment and

553 geochemistry of the Upper Pennsylvanian (Missourian) Stark shale member of the Dennis Limestone, Wabaunsee County,

554 Kansas, USA. Chem. Geol. 99, 65–82.

555 Herkat, M.; Ladjal, A., 2013. Paleobathymetry of foraminiferal assemblages from the Pliocene of the Western Sahel (North-

556 Algeria). Palaeogeography Palaeoclimatology 374, 144-163.

557 Hu, F.; Meng, Q.; Liu, Z., 2021. Mineralogy and element geochemistry of oil shales in the Lower Cretaceous Qingshankou

558 Formation of the southern Songliao Basin, northeast China: implications of provenance, tectonic setting, and

559 paleoenvironment. ACS Earth Space Chem. 5, 365−380.

560 Ji, H.; Tao, H.; Wang, Q.; Qiu, Z.; Ma, D.; Qiu, J.; Liao P., 2018. Early to middle Jurassic tectonic evolution of the Bogda

561 mountains, northwest China: evidence from sedimentology and detrital zircon geochronology. J. Asian Earth Sci., 153, 57-74.

562 Jiang, S. H.; Li, S. Z.; Somerville, I. D.; Lei, J. P; Yang, H. Y., Carboniferous-Permian tectonic evolution and sedimentation

563 of the Turpan-Hami Basin, NW China: Implications for the closure of the Paleo-Asian Ocean. J. Asian Earth Sci., 113, 644-

564 655.

565 Kidder, D. L.; Erwin, D. H., 2001. Secular distribution of biogenic silica through the phanerozoic: Comparison of silica-

23

566 replaced fossils and bedded cherts at the series level. J. GEOL. 109, 4, 509-522.

567 Korobkin, V. V.; Buslov, M. M., 2011. Tectonics and geodynamics of the western Central Asian Fold Belt (Kazakhstan

568 Paleozoides). Russian Geology and Geophysics, 52, 12, 1600-1618.

569 Kröner, S. R.; McLennan, S. M., 1985. The Continental Crust: Its Composition and Evolution; Blackwell: Oxford, 312.

570 Kroonenberg, S.B., 1992. Effect of provenance, sorting and weathering on the geochemistry of fluvial sands from different

571 tectonic and climatic environments. In Proceedings of the 29th International Geological Congress, Part A, Kyoto, Japan, 24

572 August–3 September, 69, 81.

573 Lerman, A.; Baccini, P., 1978. Lakes: Chemisty, Geology, Physics. Springer-Verlag, New York.

574 Li, C. M.; Liu, J. T.; Ni, L. B.; Fan, S. W., 2021. Characteristics of deep geological structure and petroleum exploration

575 prospect in Turpan-Hami Basin. China Petroleum Exploration, 26, 4, 44-57. (In Chinese with English abstract)

576 Li, L.; Qu, Y.Q.; Meng, Q.R.; Wu, G.L., 2011. Gravity Flow Sedimentation: Theoretical Studies and Field Identification. Acta

577 Sedimentologica Sinica 29,4, 677-688.

578 Li, RB., 2019. Filling characteristic and research significance of Permian in Tainan Depression of Tuha Basin. J. Jilin

579 Universitry (Earth science Edition) 49, 6, 1518-1528.

580 Li, Y. J.; Sun, P. C.; Liu, Z. J.; Yao, S. Q.; Xu, Y. B.; Liu, R., 2020. Geochemistry of the Permian Oil Shale in the Northern

581 Bogda Mountain, Junggar Basin, Northwest China: Implications for Weathering, Provenance, and Tectonic Setting. ACS Earth

582 and Space Chemistry4, 8, 1332-1348.

583 Li, Y. L.; Shan, X.; Gelwick, K. D.; Yu, X. H.; Jin, L. N.; Yao, Z. Q.; Li, S. L.; Yang, S. Y., 2022. Permian mountain building

584 in the bogda mountains of NW China. International Geology Review, 2048270.

585 Li, W.; Hu, J.; Li, D.; Liu, J.; Sun, Y.; Liang, J., 2007. Analysis of the late Paleozoic and Mesozoic paleocurrents and It's

586 constructional significance of the northern Bogdashan, Xinjiang. Acta Sedimentol. Sin., 25,2, 283-292.

587 Liu, D.; Zhang, C.; Yao, E.; Song, Y.; Jiang, Z.; Luo, Q., 2017. What generated the Late Permian to Triassic unconformities

588 in the southern Junggar Basin and western Turpan Basin; tectonic uplift, or increasing aridity? Palaeogeogr. Palaeoclimatol.

589 Palaeoecol., 468, 1-17.

590 Liu, D.; Kong, X.; Zhang, C.; Wang, J.; Yang, D.; Liu, X.; Wang, X.; Song, Y., 2018. Provenance and geochemistry of Lower

591 to Middle Permian strata in the southern Junggar and Turpan basins: a terrestrial record from mid-latitude NE Pangea.

592 Palaeogeogr. Palaeoclimatol. Palaeoecol., 495, 259-277.

593 Liu, G.; Zhou, D. Application of microelements analysis in identifying sedimentary environment-taking Qianjiang Formation

594 in the Jiang Han Basin as a example. Pet. Geo. Exp. 2007, 29(3), 307-311. (In Chinese with English abstract)

595 Maravelis, A. G.; Offler, R.; Pantopoulos, G.; Collins, W. J., 2021. Provenance and tectonic setting of the Early Permian

596 sedimentary succession in the southern edge of the Sydney Basin, eastern Australia. Geological J. 56, 4, 2258-2276.

597   McLennan, S. M.; Hemming, S.; McDaniel, D. K.; Hanson, G.N., 1993. Geochemical approaches to sedimentation,

598   provenance, and tectonics. Spec. Pap. Geol. Soc. Am. 284, 21−40.

599   McLennan, S. M.; Taylor, S. R.; Kröner, A., 1983. Geochemical evolution of Archean shales from South Africa I: The

600   Swaziland and Ponggola Supergroups. Precambrian Res. 22, 93– 124.

601   Mei, X.; Li, X.J.; Mi, P.P.; Zhao, L.; Wang, Z.B.; Zhong, H.X.; Yang, H.; Huang, X.T.; He, M.Y.; Xiong, W.; Zhang, Y., 2020.

602   Distribution regularity and sedimentary differentiation patterns of China seas surface sediments. Geology in China 47,5,1447-

603   1462. (in Chinese with English abstract)

604   Miao, H.; Wang, Y. B.; Guo, J. Y.; Fu, Y.; Li, J. H., 2022. Weathering correction and hydrocarbon generation and expulsion

605   potential of Taodonggou Group source rocks in Taibei Sag in Turpan‑Hami Basin. Petroleum Geology & Oilfield

606   Development in Daqing 1-11. doi:10.19597/J.ISSN.1000-3754.202204016. (In Chinese with English abstract)

607   Miao, H.; Wang, Y. B.; Guo, J. Y.; Han, W. L.; Gong, X., 2022. Evaluation of Middle Permian source rocks of the Taodonggou

608   Group in the Turpan Hami Basin. Geophysical Prospecting for Petroleum, 61, 4, 733-742. (In Chinese with English abstract)

609   Miao, H.; Wang, Y. B.; He, C.; Li, J. H.; Zhang, W.; Zhang, Y. J.; Gong, X., 2022a. Fault development characteristics and

610   reservoir control in Chengbei fault step zone,Bohai Bay Basin. Lithologic Reservoirs 34, 2, 105-115(In Chinese with an

611   English abstract).

612   Miao, H.; Wang, Y. B., Ma, Z. T.; Guo, J. Y.; Zhang, Y. J., 2022b. Generalized Deltalog R model with spontaneous potential

613   and its application in predicting total organ carbon content. Journal of Mining Science and Technology, 7, 4, 417-426. (In

614   Chinese with English abstract)

615   Miao, H.; Wang, Y. B.; Zhao, S. H.; Guo, J. Y.; Ni, X. M.; Gong, X; Zhang, Y. J.; Li, J. H., 2021. Geochemistry and Organic

616   Petrology of Middle Per-mian Source Rocks in Taibei Sag, Turpan-Hami Basin, China: Implication for Organic Matter

617   Enrichment. ACS Omega. 6,47, 31578-31594.

618   Miao, J. Y.; Zhou, L. F.; Deng, K.; Li, J. F.; Han, Z. Y.; Bu, Z. Q., 2004. Organic Matters from Middle Permain Source rocks

619   of Northern Xinjiang and Their Relationships with Sedimentary environments. Geochemica. 6,551-560. (In Chinese with

620   English abstract)

621   Nesbitt, H. W.; Nesbitt, G. M. Prediction of some weathering trends of plutonic and volcanic rocks based on thermodynamic

622   and kinetic considerations. Geochim. Cosmochim. Acta. 1984, 48(7), 1523-1534.

623   Nesbitt, H. W., Young, G. M., 1984. Prediction of some weathering trends of plutonic and volcanic rocks based on

624   thermodynamic and kinetic considerations. Geochim. Cosmochim. Acta. 48, 7, 1523-1534.

625   Novikov, I. S., 2013. Reconstructing the stages of orogeny around the Junggar basin from the lithostratigraphy of Late

626   Paleozoic, Mesozoic, and Cenozoic sediments. Russian Geology and Geophysics. 54, 2, 138-152.

627   Obrist-Farner, J.; Yang, W.; Hu, X. F., 2015. Nonmarine time-stratigraphy in a rift setting: an example from the Mid-Permian

628   lower Quanzijie low-order cycle Bogda Mountains, NW China. J. Palaeogeogr., 4, 1, 27-51.

629   Pinto, L.; Munoz, C.; Nalpas, T.; Charrier, R, 2010. Role of sedimentation during basin inversion in analogue modelling.

630   Journal of Structural Geology, 32, 4, 554-565.

631   Rollinson, H. R., 1993. Using Geochemical Data: Evaluation, Presentation, Interpretation; Longman Scientific Technical:

632   New York.

633   Rosenthal, Y.; Lam, P.; Boyle, E. A.; Thomson, J., 1995. Authigenic cadmium enrichments in suboxic sediments: precipitation

634   and postdepositional mobility - sciencedirect. Earth & Planetary Science Letters 132, 1-4, 99-111.

635   Roser, B. P.; Korsch, R. J., 1988. Provenance Signatures of Sandstone-mudstone suites determined using discriminant

636   functiom analysis of major-element data. Chem. Geol. 67, 119– 139.

637   Ross, Daniel J.K., Bustin, R. M., 2009. Investigating the use of sedimentary geochemical proxies for paleoenvironment

638   interpretation of thermally mature organic-rich strata: Examples from the Devonian–Mississippian shales, Western Canadian

639   Sedimentary Basin. Chem. Geol. 260, 1–19.

640   Schoepfer, S. D.; Shen, J.; Wei, H. Y.; Tyson, Richard V.; Ingall, E.; Algeo, T. J., 2015. Total organic carbon, organic

641   phosphorus, and biogenic barium fluxes as proxies for paleomarine productivity. Earth Sci. Rev. 149, 23–52.

642   Shao L, Li WH, Yuan MS (1999) Characteristic of sandstone and its tectonic implications of the Turpan Basin. Acta

643   Sedimentologica Sinica 17(3): 435–441.

644   Shao L, Stattegger K, Garbe-Schoenberg C (2001) Sandstone petrology and geochemistry of the Turpan Basin (NW China):

645   implications for the tectonic evolution of a Continental Basin. Journal of Sedimentary Research 71(1): 37–49. (In Chinese

646   with English abstract)

647   Shi, J.; Zou, Y. R.; Cai, Y. L.; Zhan, Z. W.; Sun, J. N.; Liang, T.; Peng, P. A., 2021. Organic matter enrichment of the Chang 7

648   member in the Ordos Basin: Insights from chemometrics and element geochemistry. Marine Petroleum Geology, 134, 105306.

649   Shi, Y. Q; Ji, H. C.; Yu, J. W; Xiang, P. F.; Yang, Z. B; Liu, D. D., 2020. Provenance and sedimentary evolution from the

650   Middle Permian to Early Triassic around the Bogda Mountain, NW China: A tectonic inversion responding to the

651   consolidation of Pangea. Mar. Pet. Geol. 114, 104169.

652   Shu, L.; Wang, B.; Zhu, W.; Guo, Z.; Charvet, J.; Zhang, Y., 2011. Timing of initiation of extension in the Tianshan, based on

653   structural, geochemical and geochronological analyses of bimodal volcanism and olistostrome in the Bogda Shan (NW China).

654   Int. J. Earth Sci., 100 ,7 , 1647-1663.

655   Song, J.; Bao, Z.; Zhao, X. M.; Gao, Y. S.; Song, X. M.; Zhu, Y. Z.; Deng, J.; Liu, W.; Wang, Z. C.; Ming, C. D.; Meng, Q.

656   K.; Zhang, L.; Mao, S. W.; Zhang, Y. L.; Yu, X.; Wei, M. Y., 2018. Sedimentology and geochemistry of Middle–Upper Permian

657   in northwestern Turpan–Hami Basin, China: Implication for depositional environments and petroleum geology. Energy

658   Exploration & Exploitation 36,4 , 910-941.

659 Sun, G. ; Liu, Y., 2009. The preliminary analysis of the uplift time of Bogda Mountain, Xinjiang, Northwest China. Acta
660 Sedimentol. Sin., 27, 3, 487-491.

661 Tang, W.; Zhang, Z.; Li, J.; Li, K.; Chen, Y.; Guo Z. 2014. Late Paleozoic to Jurassic tectonic evolution of the Bogda area
662 (northwest China): evidence from detrital zircon U–Pb geochronology. Tectonophysics, 626, 144-156.

663 Taylor, S. R.; Mclennan, S. M., 1985. The continental crust: Its composition and evolution. Blackwell Science Publications,
664 Oxford.

665 Thorpe, C. L.; Law, G. T. W.; Boothman, C.; Lloyd, J. R.; Burke, I. T.; Morris, K.; 2012. The Synergistic Effects of High
666 Nitrate Concentrations on Sediment Bioreduction. Geomicrobiol. J. 29, 5, 484-493.

667 Tian, J.Q.; Liu, J.Z.; Zhang, Z.B.; Cong, F.Y., 2017. Hydrocarbon-generating potential, depositional environments, and
668 organisms of the Middle Permian Tarlong Formation in the Turpan-Hami Basin, northwestern China. GSA Bulletin 129, 9-
669 10, 1252–1265.

670 Tribovillard, N., Algeo, T. J., Baudin, F., Riboulleau, A., 2012. Analysis of marine environmental conditions based on
671 molybdenum–uranium covariation—applications to Mesozoic paleoceanography. Chem. Geol. 324,46–58.

672 Tribovillard, N.; Algeo, T. J.; Lyons, T.; Riboulleau, A., 2006. Trace metals as paleoredox and paleoproductivity proxies: an
673 update. Chemical Geology 232, 1–2, 12–32.

674 Trbovillard, N. P.; Desprairies, A; Lallier-verges, E.; Bertrand, P.; Moureau, N.; Ramdani, A.; Ramanampiso, L., 1994.
675 Geochemical study of organic-matter rich cycles from the Kimmeridge Clay Formation of Yorkshire (UK): productivity versus
676 anoxia. Palaeogeography, Palaeoclimatology, Palaeoecology, 108,1-2,165-181.

677 Wartes, M. A.; Carroll, A. R.; Greene, T. J., 2002. Permian sedimentary record of the Turpan-Hami basin and adjacent regions,
678 northwest China: Constraints on postamalgamation tectonic evolution. Geological Society of America Bulletin, 114,2, 131-
679 152.

680 Wang, A., Wang, Z., Liu, J., Xu, N., Li, H., 2021. The Sr/Ba ratio response to salinity in clastic sediments of the Yangtze River
681 Delta. Chem. Geol. 559, 119923.

682 Wang, L., 1996. Sediment flux and mechanism for the uplifting of the mountain system around the Junggar inland basin
683 Sediment. Geol. Tethyan Geol., 16, 3, 39-46.

684 Wang, J.; Cao, Y. C.; Wang, X. T.; Liu, K. Y.; Wang, Z. K.; Xu, Q. S.,2018. Sedimentological constraints on the initial uplift
685 of the West Bogda Mountains in Mid-Permian. Sci. Rep. 8, 1453.

686 Wang, J.; Wu, C.; Li, Z.; Zhu, W.; Zhou, T.; Wu, J.; Wang, J., 2018. The tectonic evolution of the Bogda region from Late
687 Carboniferous to Triassic time: evidence from detrital zircon U–Pb geochronology and sandstone petrography. Geol. Mag.
688 155, 5, 1063-1088.

689 Wang, J.; Wu, C.; Zhou, T.; Zhu, W.; Zhou, Y.; Jiang, X.; Yang, D., 2019. Source-to-Sink analysis of a transtensional rift Basin

27

690   from syn-rift to uplift stages. J. Sediment. Res. 89, 4, 335-352.

691   Wang, J. L.; Wu, C. D.; Zhou, T. Q.; Zhu, W.; Li, X. Y.; Zhang, T., 2019. Source and sink evolution of a Permian–Triassic

692   rift–drift basin in the southern Central Asian Orogenic Belt: Perspectives on sedimentary geochemistry and heavy mineral

693   analysis. Journal of Asian Earth Sciences 181, 103905.

694   Wang, Y., 2019. Mixed Sedimentary Characteristics and Pattern of the Fan Delta in the Middle Permian Taerlanggou

695   Profile,Xinjiang Province Acta Sedimentologica Sinica, 37, 5, 922-933. (In Chinese with English abstract)

696   Wang, Z. W.; Yu, F.; Wang, J.; Fu, X. G.; Chen, W. B.; Zeng, S. Q.; Song, C. Y., 2021. Palaeoenvironment evolution and

697   organic matter accumulation of the Upper Triassic mudstone from the eastern Qiangtang Basin (Tibet), eastern Tethys. Marine

698   and Petroleum Geology 130, 105113.

699   Wronkiewicz, D. J.; Condie, K. C., 1987. Geochemistry of archean shales from the witwatersrand supergroup, south Africa:

700   Source-area weathering and provenance. Geochimica Cosmochimica Acta 51, 9, 2401-2416.

701   Wei, H.; Chen, D. Z.; Wang, J. G.; Yu, H.; Tucker, M. E., 2012. Organic accumulation in the lower Chihsia Formation (Middle

702   Permian) of South China: Constraints from pyrite morphology and multiple geochemical proxies. Palaeogeogr. Palaeoclimatol.

703   Palaeoecol. 353, 73-86.

704   Wei, X.X., 2015. Middle-Late Permian fossil woods from Northern Tuha Basin: Implications for Palaeoclimate. Master,

705   Wuhan: China university of Geosciences. (In Chinese with English abstract)

706   Wu, C.; Li, H. W.; Sheng, S. Z.; Chen, T.; Shi, X. F.; Jiang, M. L., 2021. Characteristics and main controlling factors of

707   hydrocarbon accumulation of Permian-Triassic in Lukeqin structural zone, Tuha Basin. China Petroleum Exploration 26, 4,

708   137-148. (In Chinese with English abstract)

709   Xiong, X. H.; Xiao, J. F., 2011. Geochemical Indicators of Sedimentary Environments—A Summary. Earth and Environment

710   39, 3, 405-414. (In Chinese with English abstract)

711   Xu, C. ; Shan, X. L. ; Lin, H. M .; Hao, G. L.; Liu, P .; Wang, X. D.; Shen, M. R. ; Rexiti, Y. ; Li, K.; Li, Z. S.; Wang, X. M.;

712   Du, X. D.; Zhang, Z.W.; Jia, P. M.; He, W. T., 2022. The formation of early Eocene organic-rich mudstone in the western

713   Pearl River Mouth Basin, South China: Insight from paleoclimate and hydrothermal activity. International Journal of Coal

714   geology 253, 103957.

715   Xu, H.Y., 2022. Characteristics of Permian Dark Fine-Grained Sedimentary rocks and their shale oil and gas Sigificance in

716   the Northern Margin of Turpan-Hami Basin. Master, Xi'an: Chang'an University. (In Chinese with English abstract)

717   Yang, Y.; Song, C.; He, S., 2015. Jurassic tectonostratigraphic evolution of the Junggar basin, NW China: a record of Mesozoic

718   intraplate deformation in Central Asia. Tectonics 34, 1, 86-115.

719   Yang, W.; Feng, Q.; Liu, Y.Q.; Tabor, N.; Miggins, D.; Crowley, J.L.; Lin, J.Y.; Thomas, S., 2010. Depositional environments

720   and cyclo- and chronostratigraphy of uppermost Carboniferous–Lower Triassic fluvial–lacustrine deposits, southern Bogda

721   Mountains, NW China — A terrestrial paleoclimatic record of mid-latitude NE Pangea. Global and Planetary Change, 73,

722   2010, 15-113.

723   You, J.; Liu, Y.; Zhou, D.; Zheng, Q.; Vasichenko, K.; Chen, Z., 2019. Activity of hydrothermal fluid at the bottom of a lake

724   and its influence on the development of high-quality source rocks: Triassic Yanchang Formation, southern Ordos Basin, China.

725   Australian Journal of Earth Sciences 67, 1, 115-128.

726   Yu, Y.; Cai, H.L.; Yin, T.J.; Zhang, X.Q.; Xu, H.; Huang, Y.R.; Cao, T.T., 2022. Sedimentary Characteristics and Depositional

727   Model of Lacustrine Gravity Flow Deposits: A case study of the Cretaceous Pointe Indienne Formation of Block A, Lower

728   Congo Basin. Acta Sedimentologica Sinica 2022, 40, 1, 34-46.

729   Zhang, C.; He, D.; Wu, X.; Shi, X.; Luo, J.; Wang, B.; Yang, G; Guan, S.; Zhao, X., 2006. Formation and evolution of

730   multicycle superimposed basins in Junggar Basin. China Petrol. Explor. 11, 1, 47-58.

731   Zhang, K. ; Song, Y. ; Jiang, S. ; Jiang, Z. X. ; Jia, C. Z. ; Huang, Y. Z.; Wen, M .; Liu, W. W .; Xie, X. L.; Liu, T. L.; Wang,

732   P. F.; Shan, C. A.; Wu, Y. H., 2019. Mechanism analysis of organic matter enrichment in different sedimentary backgrounds:

733   A case study of the Lower Cambrian and the Upper Ordovician-Lower Silurian, in Yangtze region. Mar. Petrol. Geol. 99,

734   488–497.

735   Zhang, S.; Liu, C.; Bai, J.; Wang, J.; Ma, M.; Guan, Y.; Peng, H., 2019. Provenance variability of the Triassic strata in the

736   Turpan-Hami basin: detrital zircon record of Indosinian tectonic reactivation in eastern Tianshan. Acta Geol. Sin. 93, 6, 1850-

737   1868.

738   Zhang, S. C.; Zhang, B. M.; Bian, L. C.; Jing, Z. J.; Wang, D. R.; Zhang, X. Y.; Gao, Z. Y.; Chen, J. F., 2005. Development

739   constraints of marine source rocks in China. Earth Sci. Frontiers 12, 3, 39-48. (In Chinese with English abstract)

740   Zhao, R.; Zhang, J. Y.; Zhou, C. M.; Zhang, Z. J.; Chen, S.; Stockli, D.F.; Olariu, C.; Steel, R.; Wang, H., 2020. Tectonic

741   evolution of Tianshan-Bogda-Kelameili mountains, clastic wedge basin infill and chronostratigraphic divisions in the source-

742   to-sink systems of Permian-Jurassic, southern Junggar Basin. Mar. Petrol. Geol. 114, 104200.

743   Zhao, B. S.; Li, R. X.; Qin, X. L.; Wang, N.; Zhou, W. ; Khaled, A .; Zhao, D.; Zhang, Y. N.; Wu, X. L.; Liu, Q., 2021.

744   Geochemical characteristics and mechanism of organic matter accumulation of marine-continental transitional shale of the

745   lower permian Shanxi Formation, southeastern Ordos Basin, north China. Journal of Petroleum Science and Engineering, 205,

746   108815.

747   Zhu, Q. M.; Lu, L. F.; Pan A. Y.; Tao, J. Y.; Ding, J. H.; Liu, W. L.; Li, M. W., 2021. Sedimentary environment and organic

748   matter enrichment of the Lower Cambrian Niutitang Formation shale, western Hunan Province, China. Petroleum Geology

749   & Experiment 43, 5, 797-854. (In Chinese with English abstract)

750   Zhu, X.; Wang, B; Chen, Y.; Liu, H. S., 2019. Constraining the Intracontinental Tectonics of the SW Central Asian Orogenic

751   Belt by the Early Permian Paleomagnetic Pole for the Turfan-Hami Block. Journal of Geophysical Research-solid earth, 124,

752   12, 12366-12387.

753

30

Appendix

Table.1 Mineral composition of Taodonggou Group mudstone in YT1 well

Samples	Depth/m	Minerals content（%）							
		Quartz	K-fledspar	Plagioclace	Calcite	Siderite	Pyrite	Barite	Clay
YT1-1	6084	29.4	0.7	1.8	23.7	/	/	13.3	31.1
YT1-2	6092	30.1	1.1	5.4	26.9	/	/	2.1	34.4
YT1-3	6102	41.9	/	2.5	18.1	/	/	3.2	34.3
YT1-4	6113	35.7	0.5	2.9	10.8	/	/	2.8	47.3
YT1-5	6122	40.5	0.1	2.7	19.4	/	/	4.6	32.7
YT1-6	6129	39.2	0.6	2.1	19.7	/	/	4	34.4
YT1-7	6136	27.9	0.3	0.8	42.8	/	/	4.3	23.9
YT1-8	6140	31.2	0.6	0.6	22.1	/	/	5.6	39.9
YT1-9	6143	34	0.4	0.2	14	/	/	4.5	46.9
YT1-10	6144.7	33.6	2.1	3.7	11.4	2.1	2.8	3.5	40.8
YT1-11	6145.3	37	/	3.7	10.6	1.4	/	2.1	45.2
YT1-12	6145.8	38.4	1.7	2.2	12.5	/	/	3.1	42.1
YT1-13	6147	37.9	/	/	1	/	1.4	1.2	58.5
YT1-14	6151	59.2	0.5	0.2	1.3	/	2.1	/	36.7
YT1-15	6154	21.8	0.8	0.8	1.8	/	/	3.9	70.9
YT1-16	6161	17.2	2.3	4.8	35.4	2	/	5	33.3

Table. 2 Major elements of Taodonggou Group mudstone in well YT1

Samples	Depth/m	Content/%										CIA	P/Ti	K_2O/Al_2O_3
		SiO_2	CaO	Al_2O_3	Fe_2O_3	K_2O	TiO_2	Na_2O	MgO	P_2O_5	MnO			
YT1-1	6084	43.79	19.05	11.65	5.32	3	1.35	1.15	1.1	0.9	0.3	68.71	0.49	0.26
YT1-2	6092	54.32	14.01	14.96	6.74	3.39	1.37	1.5	1.34	0.29	0.15	70.1	0.15	0.23
YT1-3	6102	56.63	14.36	11.66	5.42	3.38	1.24	1.23	1.36	0.16	0.19	66.63	0.09	0.29
YT1-4	6113	56.92	7.38	17.52	7.93	4.2	1.28	1.22	1.55	0.21	0.14	72.55	0.12	0.24
YT1-5	6122	51.15	12.62	15.25	7.55	3	1.33	1.2	1.15	0.3	0.34	73.85	0.17	0.20
YT1-6	6129	62.28	4.49	16.07	5.93	3.5	1.15	1.68	0.8	1.17	0.12	70.08	0.74	0.22
YT1-7	6136	52.44	9.31	16.57	8.63	2.54	1.5	1.55	0.66	0.37	0.34	74.57	0.18	0.15
YT1-8	6140	55.37	3.01	21.11	9.64	2.63	1.42	1.5	0.49	0.15	0.24	78.92	0.08	0.12
YT1-9	6143	60.24	2.76	21.27	8.73	1.92	1.76	0.84	0.36	0.23	0.22	85.5	0.09	0.09
YT1-10	6144.7	61.08	2.75	24.16	7.54	0.99	1.82	0.3	0.36	0.21	0.06	93.83	0.08	0.04
YT1-11	6145.3	61.02	2.94	25.39	6.84	0.59	1.84	0.31	0.36	0.26	0.06	95.45	0.10	0.02
YT1-12	6145.8	60.32	5.41	21.32	7.29	0.72	1.85	0.34	0.32	0.21	0.06	93.84	0.08	0.03
YT1-13	6147	60.76	1.83	25.75	7.68	0.68	1.95	0.19	0.35	0.25	0.05	96.07	0.09	0.03
YT1-14	6151	70.11	2.44	12.83	7.28	0.97	1.31	0.34	0.27	0.15	0.05	88.59	0.09	0.08
YT1-15	6154	49.39	1.92	25.41	12.25	2.84	2.87	1.57	0.46	0.15	0.06	80.97	0.04	0.11
YT1-16	6161	43.11	9.56	18.04	14.17	2.83	4.22	1.9	0.77	1.03	0.25	73.12	0.18	0.16

Table.3 Characteristics of Trace elements in Taodonggou Group mudstone

Samples		YT1-1	YT1-2	YT1-3	YT1-4	YT1-5	YT1-6	YT1-7	YT1-8	YT1-9	YT1-10	YT1-11	YT1-12	YT1-13	YT1-14	YT1-15	YT1-16
Depth/m		6084	6092	6102	6113	6122	6129	6136	6140	6143	6144.7	6145.3	6145.8	6147	6151	6154	6161
	Be	0.952	1.12	1.67	1	1.52	1.26	1.74	2.17	1.79	1.31	1.35	1.42	0.711	1.77	2.05	1.55
	Sc	9.02	11.9	15.5	11.7	13.6	13.1	15.6	16.2	21.2	11.4	13.2	12.3	7	24	26	17.6
	V	87.3	64.2	72	59.5	106	89.2	100	88.5	88.7	122.3	114.6	131.6	177	145	124	199
	Cr	27.4	21.2	31.8	27.3	40.1	43	40.1	45.1	54.8	48.5	47.6	44.5	43	63	51	40.2
	Co	9.46	12.4	14.9	13.3	11.9	12.6	13.7	18.2	27.6	22.3	21.7	20.6	18.7	24.8	36.9	30.4
	Ni	25.5	27.8	36.7	32.5	32.6	33.2	37.8	37.2	47.5	36.8	35.7	34.6	27.3	41.7	55.4	17.9
	Cu	34.2	33.1	44.8	34.6	51.2	41.8	39.9	50.8	48.9	52.6	50.3	51.4	57.3	55.8	64.4	71.2
	Zn	125	79	92.4	96.1	69.8	90.4	74.4	67.9	78.7	64.6	63.2	65.8	44.1	70.4	114	218
Content/(µg.g⁻¹)	Ga	17.81	20.1	23.3	19	24.8	21.9	15.1	13.2	16.1	14.5	12.7	13.7	7.14	12.7	19.2	17.3
	Rb	54.5	64.6	73.5	50.4	60	33.5	33.9	16	17.9	15.6	14.6	14.6	13.6	14.2	21	20.7
	Sr	758	357	420	422	291	414	269	151	199	214	244	224	63.9	126	263	393
	Mo	1.29	0.661	0.866	1.24	1.09	1.44	1.17	1.23	2.68	3.02	2.88	3.14	3.86	2.14	1.18	1.28
	Ba	483.83	735.7	633	547.28	159.24	547.66	326.49	465.2	565	503	516	505	427	254	303.56	424.35
	B	46.31	71.3	81.4	67.4	64.5	55.4	60.2	41.3	49.6	44.6	52.6	41.4	41.5	39.7	56.2	54.1
	Th	9.16	6.03	7.31	6.43	8.38	12.4	10.3	10.4	10	9.12	8.33	8.86	6.17	7.32	9.96	3.13
	U	2.13	1.8	1.83	2.14	1.66	3.1	3.17	2.43	2.06	3.1	3.06	2.89	3.2	2.66	2.42	0.73
	Zr	82.7	99.3	124	97.1	107	112	123	132	162	128.8	130.2	123.6	70.8	130.4	192	215
	Hf	2.6	3.77	4.29	3.51	3.87	4.03	4.45	4.76	5.52	4.76	3.94	4.01	2.23	3.21	6.13	6.29
Sr/Ba		1.57	0.49	0.66	0.77	1.83	0.76	0.82	0.32	0.35	0.43	0.47	0.44	0.15	0.5	0.87	0.93
Ga/Rb		0.33	0.31	0.32	0.38	0.41	0.65	0.45	0.83	0.9	0.93	0.87	0.94	0.53	0.89	0.91	0.84
B/Ga		2.6	3.55	3.49	3.55	2.6	2.53	3.99	3.13	3.08	3.08	4.14	3.02	5.81	3.13	2.93	3.13
Rb/K/(10⁻⁴)		21.87	22.94	26.18	14.45	24.08	11.52	16.07	7.32	11.22	18.97	29.79	24.41	24.08	17.63	8.9	8.81
V/Cr		3.19	3.03	2.26	2.18	2.64	2.07	2.49	1.96	1.62	2.52	2.41	2.96	4.12	2.3	2.43	4.95
V/(V+Ni)		0.77	0.7	0.66	0.65	0.76	0.73	0.73	0.7	0.65	0.77	0.76	0.79	0.87	0.78	0.69	0.92

Table 4 Characteristics of REE in Taodonggou Group mudstone

Samples	Depth/m	Content/(μg.g^{-1})																		(La/Yb)$_N$
		La	Ce	Pr	Nd	Sm	Eu	Gd	Tb	Dy	Ho	Er	Tm	Yb	Lu	∑REE	LREE	MREE	HREE	
YT1-1	6084	31.70	57.70	6.73	28.80	5.14	1.46	5.19	0.72	3.89	0.68	2.17	0.30	2.12	0.352	146.953	124.930	17.077	4.946	10.081
YT1-2	6092	27.30	47.80	5.51	22.90	4.79	0.84	4.13	0.73	4.25	0.71	2.40	0.37	2.56	0.408	124.695	103.510	15.447	5.738	7.190
YT1-3	6102	27.30	48.30	5.62	23.10	4.71	1.32	4.17	0.80	4.63	0.88	2.68	0.41	2.89	0.464	127.271	104.320	16.511	6.440	6.369
YT1-4	6113	26.40	45.60	5.20	22.20	4.37	0.96	4.09	0.68	3.88	0.72	2.35	0.36	2.56	0.408	119.783	99.400	14.705	5.678	6.953
YT1-5	6122.	32.60	62.80	7.61	31.70	6.56	1.96	5.77	0.98	5.35	0.97	2.89	0.43	2.92	0.429	162.971	134.710	21.590	6.671	7.527
YT1-6	6129	33.10	80.10	7.48	31.70	6.19	0.62	5.98	0.99	5.58	0.99	3.01	0.50	3.31	0.564	180.108	152.380	20.345	7.383	6.742
YT1-7	6136	33.50	66.40	7.70	31.20	6.19	1.18	5.46	0.91	5.24	0.96	3.05	0.49	3.18	0.454	165.914	138.800	19.936	7.178	7.102
YT1-8	6140	35.90	65.80	7.23	29.20	5.47	1.65	4.96	0.96	5.35	0.96	2.97	0.47	3.01	0.426	164.346	138.130	19.344	6.872	8.041
YT1-9	6143	39.00	73.40	9.60	40.00	7.18	1.44	5.64	1.02	5.91	1.08	3.45	0.52	3.41	0.519	192.169	162.000	22.270	7.899	7.711
YT1-10	6144.7	32.60	66.43	7.34	26.40	6.31	0.98	4.82	0.84	4.97	0.86	3.12	0.33	3.21	0.436	158.646	132.770	18.130	7.096	6.847
YT1-11	6145.3	27.90	62.23	5.23	23.20	5.42	1.04	4.46	0.92	5.41	0.88	2.88	0.44	3.02	0.423	143.453	118.560	17.880	6.763	6.228
YT1-12	6145.8	30.20	65.60	5.64	25.40	5.93	1.02	5.01	0.47	4.54	0.91	2.94	0.46	3.01	0.501	151.631	126.840	5.531	6.911	6.764
YT1-13	6147	8.84	16.80	1.75	6.90	1.39	0.30	1.32	0.27	1.87	0.39	1.27	0.22	1.67	0.265	43.247	34.290	5.531	3.426	3.569
YT1-14	6151	39.40	73.60	8.64	33.60	4.22	1.84	4.32	1.21	5.83	1.03	3.42	0.43	2.98	0.392	180.912	155.240	5.531	7.222	8.914
YT1-15	6154	52.60	105.00	12.30	50.80	9.09	2.45	7.65	1.25	7.14	1.16	3.86	0.57	3.62	0.510	257.997	220.700	28.740	8.557	9.796
YT1-16	6161	39.70	85.70	11.10	52.10	9.76	2.29	8.33	1.34	7.47	1.25	3.75	0.52	3.39	0.502	227.206	188.600	30.440	8.166	7.895

761   LREE = La + Ce + Pr + Nd; MREE = Sm + Eu + Gd + Tb + Dy + Ho; HREE = Er + Tm + Yb + Lu; (La/Yb)$_N$ = (La/Yb)/(La/Yb)$_{chondrite}$